# Applied Research Laboratory

(4)





Technical Report

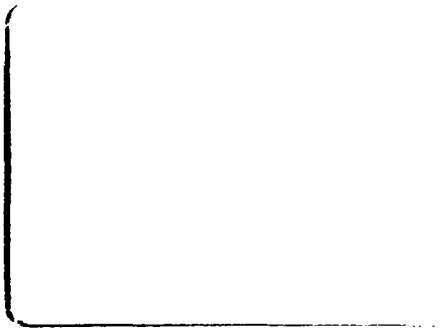



PENNSTATE

1855

The Pennsylvania State University
APPLIED RESEARCH LABORATORY
P.O. Box 30
State College, PA 16804

# SYSTEM LOSS DUE TO FREQUENCY LIMITING OF BOTTOM BOUNCES

by

M. P. Daily and D. F. McCammon

Technical Report No. TR 88-003

May 1988



Supported by:
Naval Sea Systems Command

L. R. Hettche, Director
Applied Research Laboratory

Unclassified
SECURITY CLASSIFICATION OF THIS PAGE

# REPORT DOCUMENTATION PAGE

| | |
|---|---|
| 1a. REPORT SECURITY CLASSIFICATION<br>Unclassified | 1b. RESTRICTIVE MARKINGS |
| 2a. SECURITY CLASSIFICATION AUTHORITY | 3. DISTRIBUTION / AVAILABILITY OF REPORT<br>Unlimited |
| 2b. DECLASSIFICATION / DOWNGRADING SCHEDULE | |
| 4 PERFORMING ORGANIZATION REPORT NUMBER(S) | 5 MONITORING ORGANIZATION REPORT NUMBER(S) |
| 6a NAME OF PERFORMING ORGANIZATION<br>Applied Research Laboratory<br>Penn State University<br>6b. OFFICE SYMBOL (*If applicable*)<br>ARL | 7a. NAME OF MONITORING ORGANIZATION<br>Naval Sea Systems Command<br>Department of the Navy |
| 6c. ADDRESS (*City, State, and ZIP Code*)<br>P. O. Box 30<br>State College, PA 16804 | 7b. ADDRESS (*City, State, and ZIP Code*)<br>Washington, DC 20362 |
| 8a. NAME OF FUNDING / SPONSORING ORGANIZATION<br>Naval Sea Systems Command<br>8b. OFFICE SYMBOL (*If applicable*)<br>NAVSEA | 9. PROCUREMENT INSTRUMENT IDENTIFICATION NUMBER<br>N-00024-70-C-6943 |
| 8c. ADDRESS (*City, State, and ZIP Code*)<br>Department of the Navy<br>Washington, DC 20362 | 10. SOURCE OF FUNDING NUMBERS<br>PROGRAM ELEMENT NO. / PROJECT NO. / TASK NO. / WORK UNIT ACCESSION NO. |
| 11 TITLE (*Include Security Classification*)<br>System Loss Due to Frequency Limiting of Bottom Bounces (U) | |
| 12 PERSONAL AUTHOR(S)<br>M. P. Daily and D. F. McCammon | |
| 13a TYPE OF REPORT<br>thesis<br>13b. TIME COVERED<br>FROM _____ TO _____ | 14. DATE OF REPORT (*Year, Month, Day*)<br>May 1988<br>15. PAGE COUNT<br>81 |
| 16 SUPPLEMENTARY NOTATION | |

| 17 COSATI CODES | | |
|---|---|---|
| FIELD | GROUP | SUB-GROUP |
| | | |
| | | |

18. SUBJECT TERMS (*Continue on reverse if necessary and identify by block number*)
Acoustics, Acoustic Energy Loss, Underwater Acoustics; Acoustic Wave Reflection; Acoustic Wave Scattering; Noise Measurement; Sound Processing; Specular Reflection.

19 ABSTRACT (*Continue on reverse if necessary and identify by block number*)

Processing systems which incorporate rather narrow frequency windows are often used for underwater sound measurements. When sound is being received which has bounced off the rough bottom of the ocean, some of the energy being received has returned from points on the bottom which are far from the point of specular reflection between source and receiver. Some Doppler shift is associated with these off-specular reflections when compared with the specular point. In

| | |
|---|---|
| 20 DISTRIBUTION / AVAILABILITY OF ABSTRACT<br>☒ UNCLASSIFIED/UNLIMITED ☐ SAME AS RPT ☐ DTIC USERS | 21. ABSTRACT SECURITY CLASSIFICATION<br>Unlcassified |
| 22a NAME OF RESPONSIBLE INDIVIDUAL | 22b. TELEPHONE (*Include Area Code*) / 22c. OFFICE SYMBOL |

DD FORM 1473, 84 MAR 83 APR edition may be used until exhausted. All other editions are obsolete.

SECURITY CLASSIFICATION OF THIS PAGE
Unclassified

19. (continued)

this way, frequency spreading occurs. Thus, some of the energy returning from the bottom is lost, as it is outside the frequency window used by the receiver. It is the goal of this thesis to produce an approximation of this loss, to test the approximation and to understand how the loss level is affected by environmental parameters.

A theoretical approximation for the bottom loss integral is derived for the case of a stationary measurement point and an approaching source. Reflections from the hard, rougher basement are included as well as the energy returned by the overlaying sediment. The final result is compared with the calculations of a computer-based complete model, and conclusions are made concerning the validity of the model and areas for future research.

| Accession For | |
|---|---|
| NTIS GRA&I | ☑ |
| DTIC TAB | ☐ |
| Unannounced | ☐ |
| Justification | |
| By | |
| Distribution/ | |
| Availability Codes | |
| Dist | Avail and/or Special |
| A-1 | |

## ABSTRACT

Processing systems which incorporate rather narrow frequency windows are often used for underwater sound measurements. When sound is being received which has bounced off the rough bottom of the ocean, some of the energy being received has returned from points on the bottom which are far from the point of specular reflection between source and receiver. Some Doppler shift is associated with these off-specular reflections when compared with the specular point. In this way, frequency spreading occurs. Thus, some of the energy returning from the bottom is lost, as it is outside the frequency window used by the receiver. It is the goal of this thesis to produce an approximation of this loss, to test the approximation and to understand how the loss level is affected by environmental parameters.

A theoretical approximation for the bottom loss integral is derived for the case of a stationary measurement point and an approaching source. Reflections from the hard, rougher basement are included as well as the energy returned by the overlaying sediment. The final result is compared with the calculations of a computer-based complete model, and conclusions are made concerning the validity of the model and areas for future research.

# TABLE OF CONTENTS

## Table of Contents (continued)

# LIST OF TABLES

# LIST OF FIGURES

## List of Figures (continued)

# NOMENCLATURE

| | |
|---|---|
| $a$ | distance from source to point $(x, y)$ |
| $A_s$ | coefficient of sediment $x$-slope for Gaussian weighting |
| $A_b$ | coefficient of basement $x$-slope for Gaussian weighting |
| $A_1$ | coefficient of sediment $x$-slope for cosine weighting function |
| $A_2$ | coefficient of sediment $y$-slope for cosine weighting function |
| $A_3$ | coefficient of basement $x$-slope for cosine weighting function |
| $A_4$ | coefficient of basement $y$-slope for cosine weighting function |
| $\alpha_s$ | attenuation coefficient of the sediment |
| $b$ | distance from receiver to $(x, y)$ point |
| $B$ | weighting function on the bottom due to beam pattern |
| $B_s$ | coefficient of sediment $y$-slope for Gaussian weighting |
| $B_b$ | coefficient of basement $y$-slope for Gaussian weighting |
| $\beta_s$ | source bearing |
| $\beta_r$ | receiver bearing |
| $\chi$ | ratio of sediment sound speed to water sound speed at bottom |
| $c$ | distance from point directly under source to $(x, y)$ |
| $c_w$ | speed of sound in the water just above sediment |
| $c_s$ | speed of sound in sediment just above basement |
| $D$ | total dissipation due to losses in the sediment |
| $d$ | distance from point directly under receiver to $(x, y)$ |
| $\Delta f_0$ | Doppler shift at specular reflection point |

## Nomenclature (continued)

| | |
|---|---|
| $E_t$ | total energy reflected to the receiver point |
| $E_p$ | energy reflected to the receiver which it can detect |
| $\Delta f$ | half the bandwidth of the filter |
| $e$ | inverse natural logarithm of 1 |
| $f(L_1, L_2, L_3, L_4)$ | volume underneath cosine sediment weighting function limited by $L_1 < x < L_2$ $L_3 < y < L_4$ |
| $g(M_1, M_2, M_3, M_4)$ | volume underneath cosine basement weighting function limited by $M_1 < x < M_2$ $M_3 < y < M_4$ |
| $h$ | height of receiver off ocean floor |
| $h_a$ | apparent height of receiver off ocean floor |
| $l$ | path length in sediment |
| $L_s$ | system loss |
| $L_1 - L_4$ | limits in integral for sediment cosine weighting function |
| $M_1 - M_4$ | limits in integral for basement cosine weighting function |
| $P$ | shorthand for $\frac{c(\Delta f + D_{f0})}{v_s}$ |
| $\phi_1$ | azimuthal angle from source to $(x, y)$ point |
| $\phi_2$ | azimuthal angle from receiver to $(x, y)$ point |
| $R$ | horizontal range travelled by sound for specular reflection |
| $R_s$ | energy reflection coefficient off sediment/water interface |
| $R_b$ | energy reflection coefficient of sediment/basement interface |
| $\rho$ | density ratio |
| $\rho_s$ | density of the sediment |

## Nomenclature (continued)

| | |
|---|---|
| $\rho_w$ | density of the water |
| $S_{xb}$ | slope of the basement in the $x$-$z$ plane |
| $S_{xs}$ | slope of the sediment in the $x$-$z$ plane |
| $S_{yb}$ | slope of the basement in the $y$-$z$ plane |
| $S_{ys}$ | slope of the sediment in the $y$-$z$ plane |
| $\sigma_s$ | RMS roughness of sediment surface |
| $\sigma_b$ | RMS roughness of basement surface |
| $\theta_s$ | specular reflection angle at water/sediment interface |
| $\theta_b$ | specular reflection angle at sediment/basement interface |
| $\theta_1$ | angle formed by line from source to $(x, y)$ and bottom |
| $\theta_2$ | angle formed by line from receiver to $(x, y)$ and bottom |
| $\theta_w$ | angle of incidence into sediment at general $(x, y)$ point |
| $\theta_2$ | angle of incidence into basement at general $(x, y)$ point |

## ACKNOWLEDGEMENTS

I would like to thank most of all Dr. Diana F. McCammon for all the help and support she has given me in the completion of this project and all of my graduate studies here. I would also like to acknowledge the assistance of Dr. Gus Leibiger at NUSC, New London, with the full model and the slopes derivation, and Cathy Clark at Sonalysts Inc., New London.

# Chapter 1

# THE GENERAL PROBLEM

## 1.1. Introduction

A source moves through the water with velocity $v_s$ at bearing $\beta_s$ towards a receiver with speed $v_r$ and bearing $\beta_r$. Single frequency steady state sound emanating from this source travels through the water column to the bottom, where it reflects in such a way that it reaches the receiver (Figure 1, p. 9). The water column in general has a sound velocity profile which may make the angle which the sound hits the receiver, the source, and the bottom all different. The point where the sound returning from the bottom would be expected to strike if the bottom were perfectly flat is the specular point. The receiver tunes his filter so that the center of the filter is on the frequency of the sound returning from the specular point. This is also the least-time path. The sound at this specular point is, in general, Doppler shifted with respect to the sound emanating from the source by an amount $\Delta f_0$. Note also that this specular point is not necessarily equidistant from the source and receiver, since they are not necessarily at the same depth.

The bottom consists of a layer of sediment covering a hard basement (Figure 2, p. 10). At the water/sediment interface, some of the sound energy is reflected, and some is transmitted. The transmitted sound will propagate through the sediment, strike the bottom or refract, and emerge from the sediment downrange. The sediment will in general have a sound velocity profile of its own. This allows the sound transmitted into the sediment to refract before it hits the basement. The sound propagating through the sediment is attenuated by the sediment by an amount $e^{-\gamma l}$, where $\gamma$ is an absorption coefficient and $l$ is the total distance travelled in the sediment.

If the sediment is not perfectly smooth, some energy will return from reflection points different from the specular point. Sound from these points is Doppler shifted with respect to the specular point. If the receiver has a narrow filter, some of the energy may be Doppler shifted out of the frequency window of this filter, and thus cannot be detected. Obviously this represents a bias in the energy reported by the receiver system.

We can assign a probability of such a reflection occurring at a point $(x, y)$ if we calculate the slope the sediment must have to reflect energy to the receiver at that point. Assigning a probability of such a slope occurring gives us a weight to give to the energy returning from the off-specular point $(x, y)$. A similar situation exists in the basement. This probability is assumed Gaussian in slope. For instance, the probability of the basement having a slope in the $x$-$z$ plane of magnitude $S_{xb}$ is

$$\frac{e^{S_{xb}^2/\sigma_b^2}}{\sigma_b^2},$$

where $\sigma_b$ is the rms slope of the basement, which is different from the rms slope of the overlying sediment. Of course, the same formula applies to the sedimentary layer with the sediment slope $\sigma_s$ replacing the basement slope in the above equation. Thus, these probability functions reflect the roughnesses of the surfaces. It should be noted that in this model, we are dealing with energy quantities, not pressure quantities. In other words, all summing is assumed incoherent.

The source is assumed omnidirectional. The receiver may have a beam pattern associated with it. It is assumed that the beam is perfectly centered on the specular point. This beam pattern, when projected onto the bottom, will also weight the sound energy returning from an $(x, y)$ point by some function $B(x, y)$.

We will be referring to slopes on the bottom a great deal, and it is essential to have a clear understanding of them. Since we have assumed plane wave (the Kirchhoff Approximation) reflection, for energy to reach the receiver from any off-specular point, the bottom at that point must be tilted. See Figure 3, p. 11. This tilt can be broken down into slopes in the $x$-$z$ plane and slopes in the $y$-$z$ plane, termed x-slope and y-slope and denoted $S_x$ and $S_y$ respectively. They are calculated as rise over run, or $\frac{\partial h}{\partial x}$ and $\frac{\partial h}{\partial y}$, where $h$ is the height of the bottom locally. If the bottom is tilted at an angle of 15 degrees from horizontal in the $x$-$z$ plane, $S_x = \tan(15)$.

It is also important to know which angles are which. Towards that end, some explanation is given:

- $\theta_s$ is the angle of specular reflection off the sediment.
- $\theta_b$ is the angle of specular reflection off the basement.
- $\theta_w$ is the angle of incidence into the sediment at a general $(x, y)$ point.
- $\theta_r$ is the angle of sound in the sediment after it has been refracted by the water/sediment interface at a general $(x, y)$ point.
- $\theta_1$ is the angle formed by the line from the source to the $(x, y)$ point and the sediment surface (assumed flat).
- $\theta_2$ is the angle formed by the line from the receiver to the $(x, y)$ point and the sediment surface (assumed flat).
- $\phi_1$ is the azimuthal angle from the source to the $(x, y)$ point
- $\phi_2$ is the azimuthal angle from the receiver to the $(x, y)$ point

## 1.2. The System Loss Integral

Having now seen that only some of the energy reflected at the interface is picked up by the receiver, we can now formulate the total system loss associated with frequency limiting and Doppler shift. It is the ratio of energy picked up

by the receiver to the total energy which reaches the receiver location. Starting with the latter, if we integrate the energy returning to the receiver point from a differential area $dxdy$ over the whole ocean floor, we will get the total energy returned to the receiver point. In mathematical terms, this can be written

$$E_t = \int\int^{\infty} W\,dxdy,$$

where $W$ is the amount of energy reflected from the $(x, y)$ spot taking into account probabilities, reflection, transmission and reflection, absorption, and whatever else is necessary.

The energy picked up by the receiver is the sum over the whole bottom of the energy which is not rejected by the filter because of its Doppler shift. Furthermore, the energy is weighted by the beam pattern of the receiving hydrophone. In mathematical form

$$E_p = \int\int^{f} B \cdot W\,dxdy,$$

where $B$ is the projection of the beam pattern onto the bottom, and the integral is no longer over infinity but limited by frequency. The total system loss is thus

$$L_s = \frac{\int\int^{f} B \cdot W\,dxdy}{\int\int^{\infty} W\,dxdy}.$$

For the purposes of this development, it will be convenient to split this integral up into two parts

$$L_s = \frac{\int\int^{f} B \cdot W\,dxdy}{\int\int^{\infty} B \cdot W\,dxdy} \cdot \frac{\int\int^{\infty} B \cdot W\,dxdy}{\int\int^{\infty} W\,dxdy}. \tag{1}$$

Now the term on the right is strictly beam pattern dependent and the term on the left is associated with the frequency limiting. It is this term which is the topic of this thesis.

For clarity, It should be pointed out that here we are estimating system loss, not bottom loss. The two are very different. System loss is a bias in the

energy measured by a system due to some system limitations. Bottom loss is the difference between the energy incident on the bottom and the energy returned by the bottom.

## 1.3. The Assumptions

If one were to go ahead and plug exact mathematical forms for all the quantities previously discussed into (1), the resulting integrals would be very complex, and probably solvable in series form only, if at all. Looking ahead, the weighting function $W$ which represents the energy returning from an $(x, y)$ spot is going to involve at least a Gaussian probability multiplied by some dissipation function $D(x, y)$. The difficulties in integrating Gaussians to finite limits are well known, and the methods used are often involved and lack simple closed form solutions. In an attempt to keep the math manageable, I intend to solve a very specific, approximate problem in a closed form rather than attempt to solve the general, exact problem approximately using other methods. It is hoped that the result will give a good approximation to the real loss without needing a computer. However, it is noted here that these other methods do exist and further research into the possibilities they offer should be done in order to get a better understanding of the processes involved in this complex problem.

The methods used here are basically an extension of the methods of Zabal and Brill[1,2] to two layers. Most of the assumptions made by them still apply here. They are:

- No diffraction (wavelength much smaller than bottom variations)
- Acoustic path are not affected by height variations
- Bottom has isotropic and homogenous slope statistics
- No shadowing
- Weighting is Gaussian in slope

- Incoherent summing of energy reflected off the surface
- Only one bounce is important (no multiple bounces in the sediment)
- Omnidirectional receiver

Note the last restriction. We are going to restrict the scope of this study to the case of a receiver with a uniform or omnidirectional beam. That is to say that $B$ in equation (1) is equal to unity. Thus, the right hand side of equation (1), the one associated with losses due to beam pattern, has a value of unity, and the terms in the part associated with frequency loss are greatly simplified. Thus the total loss equation becomes

$$L_s = \frac{\int\int^f W\,dxdy}{\int\int^\infty W\,dxdy}. \tag{2}$$

Now we invoke a great number of simplifying assumptions which will make our integral manageable. In the end, we will test some of these assumptions for validity and see the effects of violating some others.

In order to get a grasp on the types of assumptions to make, let's now formulate our weighting function $W$. The slope probabilities are used to weight the energy returning from the $(x, y)$ spot. On the sediment, we only need to account for the (energy) reflection coefficient and the probability of the slopes associated with an $(x, y)$ point. Thus for the sediment,

$$W_s = R_s(x,y) \cdot \frac{e^{-(S_{xs}^2+S_{ys}^2)/\sigma_s^2}}{\sigma_s^2}.$$

For the basement, we need to take into account the transmission into the sediment, the dissipation through the sediment, the reflection off the basement, and the transmission back into the water as well as the probability of the slopes existing. Thus, the total energy through the sediment is

$$W_b = R_b(x,y) \cdot (1 - R_s(x,y))^2 \cdot D(x,y)\frac{e^{-(S_{xb}^2+S_{yb}^2)/\sigma_b^2}}{\sigma_b^2}.$$

The total weighting function $W$ is the sum of $W_s$ and $W_b$.

First, we assume that the water has an isovelocity profile, as will the sediment. The sediment has a different sound velocity from the water above it. As will be seen later, an isovelocity profile allows us to use straight line geometry in our calculations of angles and slopes. Second, we will assume that the source and receiver are at the same depth, which is probably not too restrictive if the water is deep and the source and receiver are near the surface. Now we can say the horizontal range travelled over the bottom from the source to the specular point is

$$R = \frac{h}{\tan(\theta_s)}.$$

We will assume that the reflection coefficients, both off the sediment and off the basement, are constant over the entire bottom. The (energy) reflection coefficient $R_b$ off the basement is chosen to be 0.25, as is used in the full model we will compare with later. It represents the reflection off a granite basement. The reflection off the sediment $R_s$ will be given by the reflection at the specular point as calculated using classical plane wave theory (Figure 2, p. 10).

$$R(x,y) = \left( \frac{\rho_s c_s \sin(\theta_w) - \rho_w c_w \sin(\theta_r)}{\rho_s c_s \sin(\theta_w) + \rho_w c_w \sin(\theta_r)} \right)^2,$$

where $\theta_w$ is the angle of incidence into the sediment at the $(x,y)$ point and is in this case the specular angle $\theta_s$. $\theta_r$ is the angle of the sound in the sediment after it has refracted. If we are below a critical angle, then $\theta_r$ at the specular point does not exist. Note that by assuming constant sound speed in the sediment, no refraction can take place in the sediment. All energy that penetrates the water/sediment interface hits the basement. In the real ocean, this is not true: if the angle of incidence is low enough, energy that penetrates into the sediment will refract before it hits the basement. Note also that if we are below a critical angle (ie $\frac{c_s}{c_w}\cos(\theta_w) \geq 1$) then $W_b$ is zero.

Likewise, we will assume that the total dissipation of sound as it travels through the sediment is constant over the whole bottom. This is the same as assuming that the total path length in the sediment is constant over the whole bottom. We will again use the value at the specular spot as the value everywhere,

$$D = 10^{-2\alpha_s \sin(\theta_b)},$$

where $\theta_b$ is the specular angle for the penetrating path. The total length traveled in the sediment is represented by $2s\sin(\theta_b)$ It is important to note that $\theta_b$ is not just $\arccos(\frac{c_w}{c_s}\cos(\theta_s))$ because of the extra range travelled in the sediment. It must be calculated independently, and the calculation is not trivial. We will see this later.

All of these assumptions are later tested using a full model that employs numerical integration of equation 2.

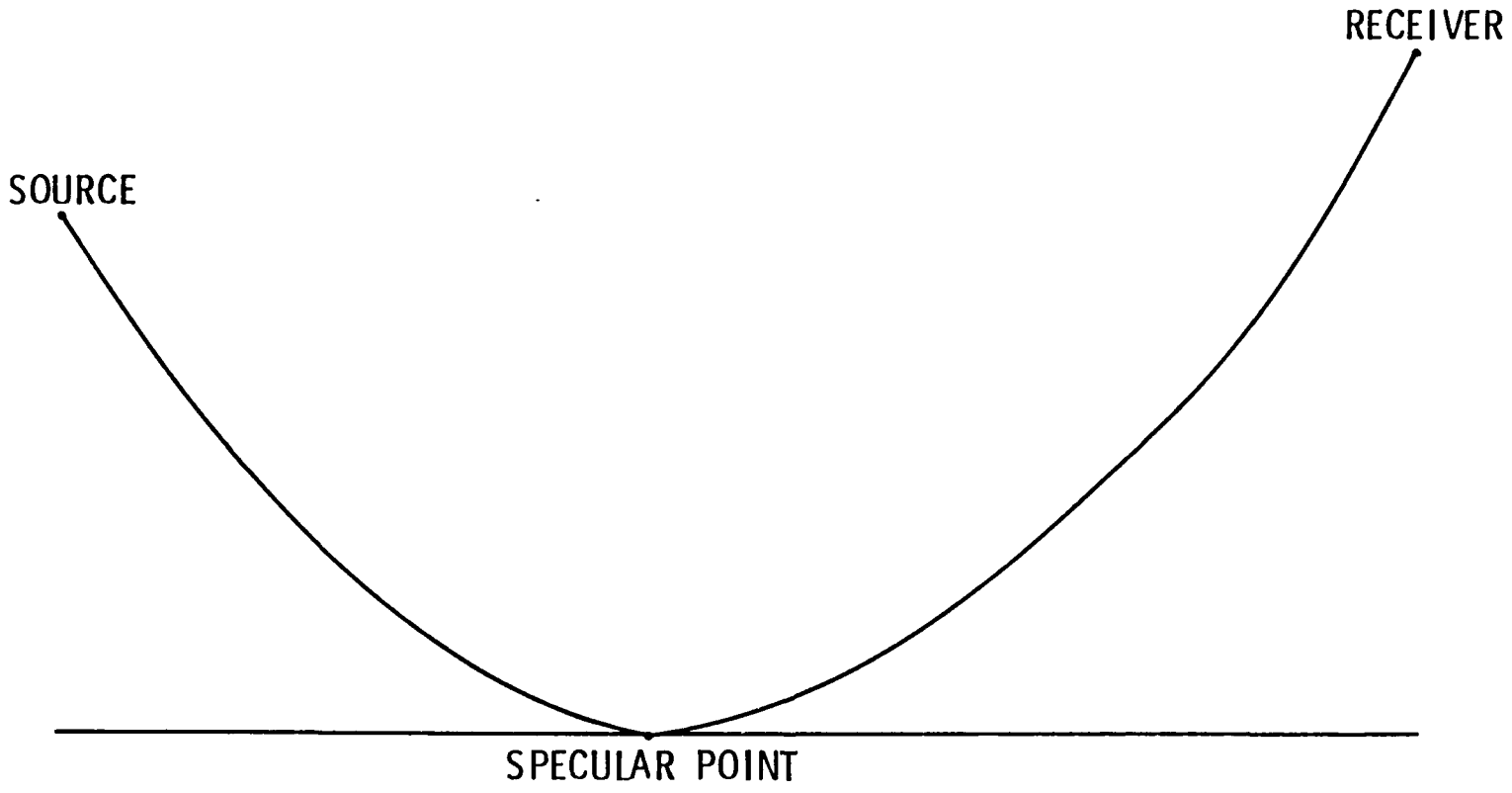


**Figure 1** **Specular Bottom Bounce Path**

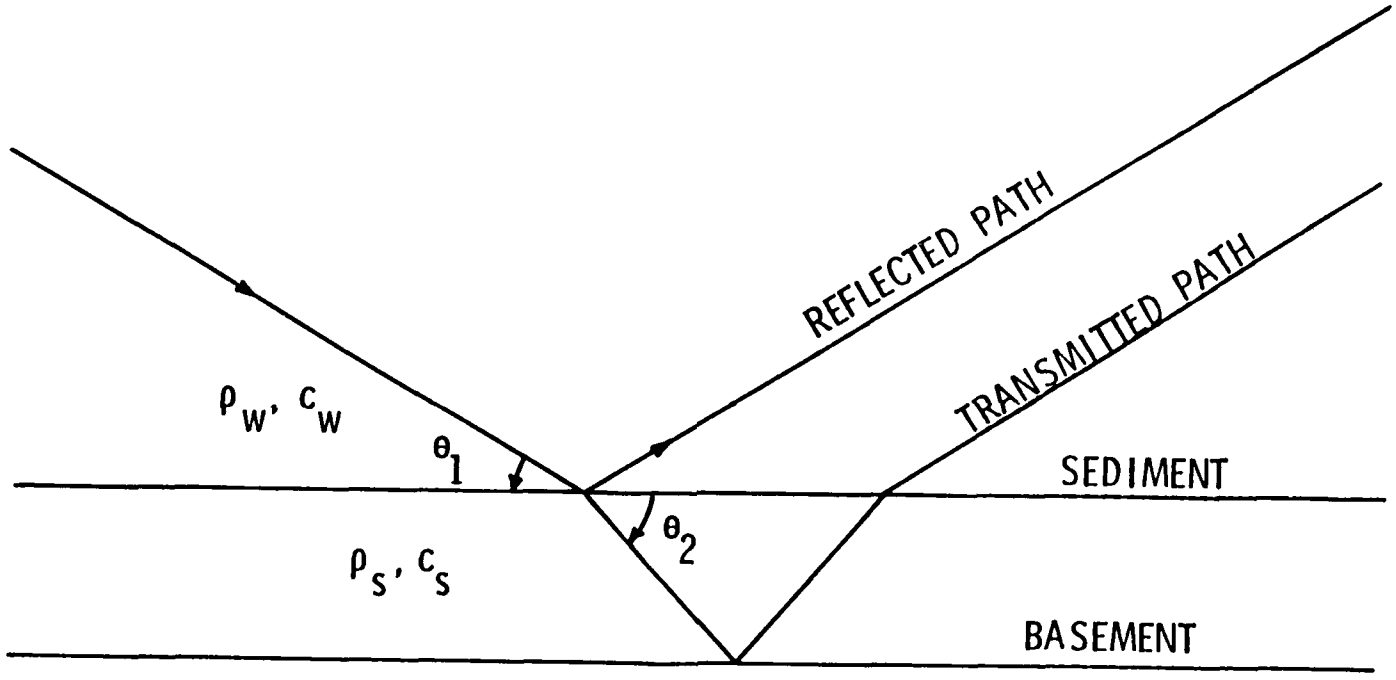


**Figure 2** **Two Layer Reflection**

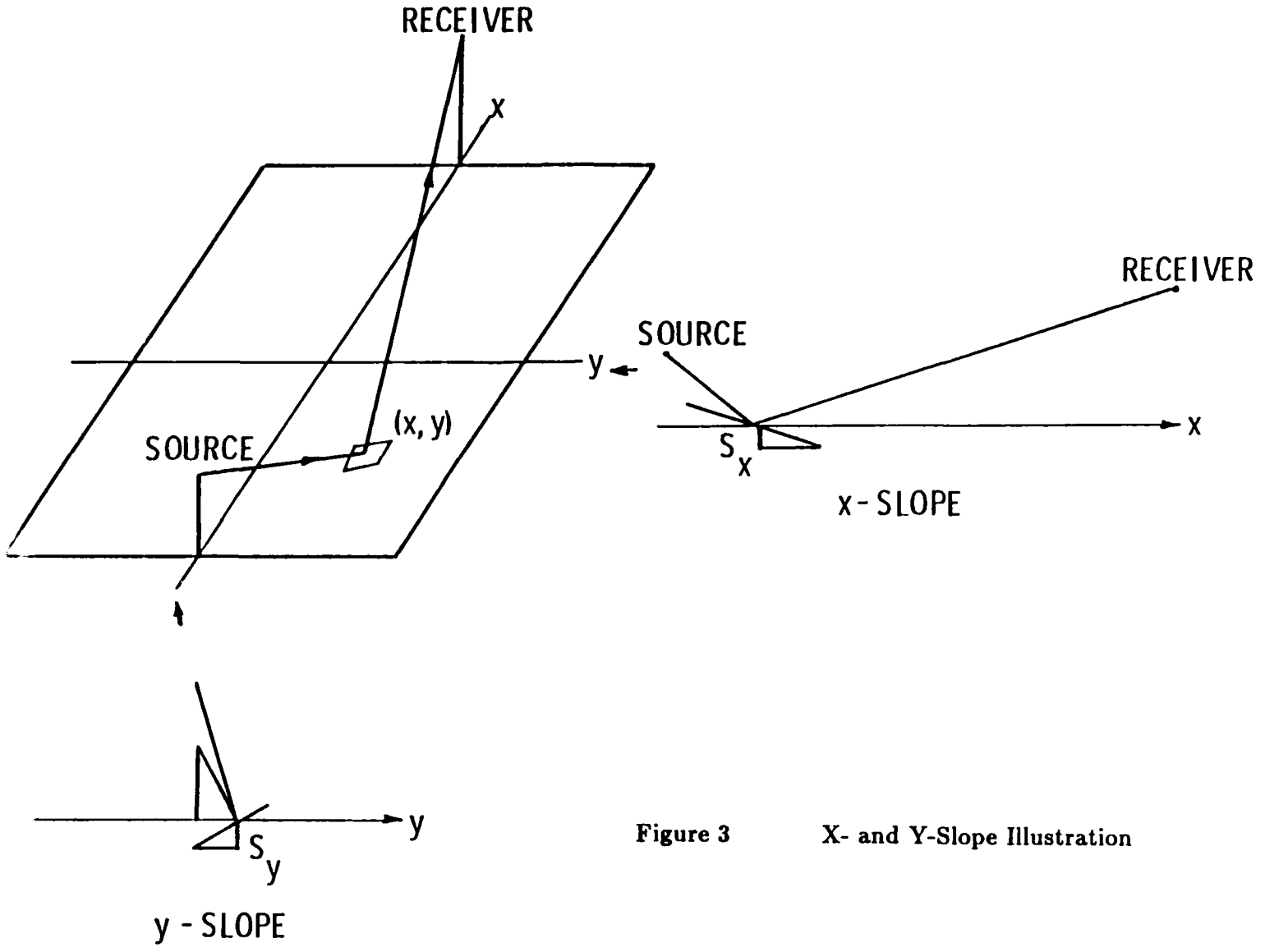


**Figure 3** X- and Y-Slope Illustration

# Chapter 2

# THE DERIVATIONS

## 2.1. Introduction

Now we will re-state the weighting function using the assumptions just made.

$$W = R_s \cdot \frac{e^{-(S_{xs}^2+S_{ys}^2)/\sigma_s^2}}{\sigma_s^2} + (1-R_s)^2 \cdot R_b \cdot D \cdot \frac{e^{-(S_{xb}^2+S_{yb}^2)/\sigma_b^2}}{\sigma_b^2}. \qquad (3)$$

where now $R_s$,$R_b$, and $D$ are not functions of $(x,y)$. In order to have any hope of integrating this function, we need to write the function strictly in terms of $(x,y)$. The slopes $S_{xs,xb}$ and $S_{ys,yb}$ are the only quantities remaining that change with the $(x,y)$ point. We are fortunate that these quantities end up being well approximated by simple linear functions of $x$ and $y$. If this were not true, the problem would be intractable.

## 2.2. The Sediment Slopes

It is shown in Appendix A that the slope in the $x$-$z$ plane necessary for specular reflection on the bottom is given by

$$S_{xs} = \frac{\cos(\theta_1)\cos(\phi_1) - \cos(\theta_2)\cos(\phi_2)}{\sin(\theta_1)+\sin(\theta_2)}, \qquad (4)$$

where the angles used are illustrated in Figure 4 on p. 24. Also from Appendix A, the slope of the bottom in the $y$-$z$ plane is given by

$$S_{ys} = \frac{\cos(\theta_1)\sin(\phi_1) + \cos(\theta_2)\sin(\phi_2)}{\sin(\theta_1)+\sin(\theta_2)}. \qquad (5)$$

Since straight line propagation is assumed, we can use side ratio relations to replace the trigonometric functions. Examination of Figure 4 (p. 24) shows that

$$\cos(\theta_1) = \frac{d}{a}, \qquad \sin(\theta_1) = \frac{h}{a},$$

$$\cos(\theta_2) = \frac{c}{b}, \qquad \sin(\theta_2) = \frac{h}{b}, \qquad (6)$$

$$\cos(\phi_1) = \frac{R+x}{d}, \qquad \sin(\phi_1) = \frac{y}{d},$$

$$\cos(\phi_2) = \frac{R-x}{d}, \qquad \sin(\phi_2) = \frac{y}{c}.$$

Starting with $S_y$, plugging equation (6) into equation (5), some simple algebra will yield the equation.

$$S_y = \frac{y}{h} = B_s \cdot y, \qquad B_s = \frac{1}{h}, \tag{7}$$

which is as simple an equation as one could hope for, a simple multiplier of $y$. Unfortunately, we are not so lucky with $S_x$. When we plug equation (6) into (4), we end up with

$$S_x = \frac{R}{h}\frac{(b-a)}{(b+a)} + \frac{x}{h}, \tag{8}$$

where

$$a = \sqrt{(R+x)^2 + h^2 + y^2},$$

$$b = \sqrt{(R-x)^2 + h^2 + y^2}.$$

We will now assume the the slope in the $x$-$z$ plane does not depend on $y$. Setting $y = 0$ in (8) still leaves us with a difficult equation. If we assume that $x^2 \ll R^2 + h^2$, we can approximate the equation (8) by a linear term

$$S_x \approx A_s \cdot x.$$

where $A_s$ will be the derivative of equation (8) with respect to $x$ evaluated at the point $x = 0$. Carrying out that derivative (Appendix B), $A_s$ is found to be

$$A_s = \frac{h}{h^2 + R^2}. \tag{9}$$

So now we can use two simple linear terms to get the slopes in the sediment in our weighting function

$$S_x \approx A_s \cdot x, \qquad S_y = B_s \cdot y. \tag{10}$$

## 2.3. The Slopes of the Basement

When calculating the slopes in the basement, we must take into account the refraction that will in general occur at the water/sediment interface (Figure 2, p. 10). Remember that we have assumed that the velocity in the sediment is constant, so the angle at which the sound hits the basement is the same as the angle that it has after it refracts the water/sediment interface. Summing up the ranges in the water and in the sediment, we get

$$R = \frac{h}{\tan(\theta_w)} + \frac{s}{\tan(\theta_r)},$$

where $\theta_w$ is the angle into the sediment and $\theta_r$ is the angle into the basement and the $(x, y)$ point. Converting tan to cos (in order to use Snell's Law)

$$\tan(\theta_w) = \frac{\sqrt{1 - \cos(\theta_w)^2}}{\cos(\theta_w)}$$

Similarly for $\tan(\theta_r)$. Using Snell's law,

$$\cos(\theta_r) = \frac{c_s \cdot \cos(\theta_w)}{c_w}$$

using the third equation to substitute in the second, and the second into the first, you would see that the resulting equation for $\theta_r$ in terms of $x$ and $y$ would be difficult. It is in fact transcendental, as is shown in Appendix C. Instead, we will take a much simpler, approximate, approach. We will replace the height of the source and receiver $h$ by an apparent height $h_a$ for calculations of slopes on the basement over the whole basement. In other words, as far as an observer on the basement can tell, the source (and receiver) are at a height $h_a$ different from $h$ due to refraction. We can then carry out the same sort of analysis as for the sediment slopes by just replacing $h$ by $h_a$ in equations (7),(8), and (10). Thus the slope in the $y$-$z$ plane on the basement is given by

$$S_{yb} = \frac{y}{h_a}. \tag{11}$$

It now remains to calculate $h_a$. We will end up with the same transcendental equation as before. Appendix C gives an approximate apparent height formula which we will use in our calculations. It is good whenever the ratio of sediment sound speed to water sound speed at the water/sediment interface is not too far from unity, which is often the case.

The slope in the $x$-$z$ plane is given by

$$S_{xb} = \frac{R}{h_a}\frac{(b-a)}{(b+a)} + \frac{x}{h_a}.$$

In the real ocean, the roughness of the basement is much greater than on the sediment. This is because the basement is made up of hard rock instead of the soft mud or clay deposited on top of it. We cannot make the small slopes approximation as we did before to get the $x$-$z$ slopes in a workable form. Using the tangent slope approximation, we would end up with equation (10) with $h$ replaced by $h_a$.

$$S_{xb} = A_b \cdot x, \qquad A_b = \frac{h_a}{h_a^2+R^2}. \tag{12}$$

Figure 5 on page 25 plots $S_{xb}$ *.vs.* $x$ using equation (12) and the "true" equation, equation (8) with $h = h_a$, $y = 0$. For convenience, the slopes have been converted to angle equivalents in degrees.

For $S_{xb}$ less than 6 degrees, we can see that the line from equation (12) and the curve from equation (8) agree quite closely. On the sediment, RMS slopes are usually between 1 and 6 degrees. Since the point where the slope equals the RMS slope of the surface corresponds to the 3 dB down point of the gaussian function, the 3 dB points of the probability function on the sediment are well matched, and the Gaussian given by $e^{-(S_{xs}/\sigma_s)^2}/\sigma_s$ and $e^{-(A_s \cdot x/\sigma_s)^2}/\sigma_s$ fall off at near the same point. Unfortunately, RMS slopes in the basement are sometimes as high

as 22 degrees [3]. We can see that the point where the line $A_b \cdot x$ crosses 0.36 (tan (22))is way off the plot of Figure 5, whereas equation (8) crosses 0.36 at about 14000 yards. As a result, the weighting function $e^{-(A_b \cdot x)^2}/\sigma_b$ falls off much too far away from the specular point compared with $e^{-(S_{xb}/\sigma_b)^2}/\sigma_b$. The frequency loss will be much too high, so this is not an acceptable approximation. We will still be using a line $S_{xb} = A_b \cdot x$. but instead of using the derivative method, we will use a two point matching technique. We will make the $S_x$ approximation match at the specular point (where it is equal to zero) and directly underneath the source. This point was not chosen arbitrarily. Examination of the full model showed that the probability function usually dies off somewhere near the source. Further, the equations are greatly simplified at this point. Thus, by matching the point where the probability vanishes, we insure that the probability function covers about the right sized area on the bottom. The slope function (8) evaluated at the point $x = R$ comes out

$$S_{xb}\,|_{x=R} = \frac{R}{h_a}\frac{\sqrt{4R^2+h_a^2}-h_a}{\sqrt{4R^2+h_a^2}+h_a} + \frac{R}{h_a}. \tag{13}$$

We will say that

$$S_{xb} = \frac{x \cdot S_{xb}|_{x=R}}{R} = A_b \cdot x, \qquad A_b = \frac{S_{xb}|_{x=R}}{R}. \tag{14}$$

## 2.4. The Weighting Function

Now looking at our integral as it stands, we see

$$\int\int \left( R_s \frac{e^{-(A_s^2x^2+B_s^2y^2)/\sigma_s^2}}{\sigma_s^2} + R_b(1-R_s)^2 D \frac{e^{-(A_b^2x^2+B_b^2y^2)/\sigma_b^2}}{\sigma_b^2} \right) dxdy. \tag{15}$$

Taking the sediment integral first, we see that the resulting integrand is a perfect Gaussian. The integral is therefore an error function. Assuming that the limits in $f$ delineate a box in the $x$-$y$ plane, we could state the final solution

in terms of error functions. However, error functions are not implemented on most calculators, or even in many computers. Furthermore, the limits may not be simple numbers, but instead describe a curve on the $x$-$y$ plane. It is thus desirable to try to get the weighting functions into a form we can integrate to obtain a closed form solution. In order to get this integrand into a form we can integrate, approximate the function

$$e^{-A_s^2 x^2}$$

where the RMS slope has been absorbed into $A_s$, so that now

$$A_s = \frac{h}{h^2 + R^2} \cdot \frac{1}{\sigma_s},$$

by a cosine function

$$e^{-A_s^2 x^2} = \begin{cases} \cos(A_1 \cdot x); & \frac{-\pi}{2A_1} \leq x \leq \frac{\pi}{2A_1} \\ 0; & \text{elsewhere} \end{cases}. \tag{16}$$

See Figure 6 on page 26. The two functions have a unity value at the point $x = 0, y = 0$. They have the same behavior away from the specular. Because the cosine "bulges" more than the exponential, they can be matched at one other point, which for simplicity will be picked as the point where they equal $1/e$. Setting the left hand side of (16) equal to $1/e$, we find $x = 1/A_s$. Therefore

$$\cos(A_1/A_s) = 1/e,$$

or

$$A_1 = A_s \cdot \arccos(1/e). \tag{17}$$

Doing the same thing for the term involving $y$, we get

$$A_2 = B_s \cdot \arccos(1/e), \tag{18}$$

where

$$B_s = \frac{1}{\sigma_s \cdot h}.$$

So we can now approximate our Gaussian weighting function on the sediment

$$\frac{e^{-A_s^2x^2-B_s^2y^2}}{\sigma_s^2},$$

by the integrable function

$$A_1A_2\cos(A_1x)\cos(A_2y). \tag{19}$$

Note that the approximate weighting function is defined to have a value 0 for $\mid x \mid \geq \frac{\pi}{2A_1}$ or $\mid y \mid \geq \frac{\pi}{2A_2}$. Thus, the new weighting function has values only within a box on the $(x,y)$ plane. This must be remembered later when we integrate so that the limits do not take the weighting function outside the defined area. The variables $A_1$ and $A_2$ are necessary to normalize the new weighting function, and take the place of $\sigma_s^2$ in the denominator of equation (15).

An exactly analogous thing is done for the basement functions with the result

$$\frac{e^{-A_b^2x^2-B_b^2y^2}}{\sigma_b^2} \approx A_3A_4\cos(A_3x)\cos(A_4y), \tag{20}$$

where

$$A_b = \frac{S_{xb}\mid_{x=R}}{R\sigma_b},$$

$$B_b = \frac{1}{h_a\sigma_b},$$

$$A_3 = A_b\arccos(1/e),$$

$$A_4 = B_b\arccos(1/e).$$

If we now define the integral of (19) over both $x$ and $y$

$$\int_{L_1}^{L_2}\int_{L_3}^{L_4}\cos(A_1x)\cos(A_2y)dxdy$$

as a function $f(L_1,L_2,L_3,L_4)$ for the sediment and $g(M_1,M_2,M_3,M_4)$ for the basement, then the loss equation becomes.

$$L_s = \frac{R_sf(L_1,L_2,L_3,L_4) + R_b(1-R_s)^2Dg(M_1,M_2,M_3,M_4)}{R_sf(\frac{-\pi}{2A_2},\frac{\pi}{2A_2},\frac{-\pi}{2A_1},\frac{\pi}{2A_1}) + R_b(1-R_s)^2Dg(\frac{-\pi}{2A_4},\frac{\pi}{2A_4},\frac{-\pi}{2A_3},\frac{\pi}{2A_3})}. \tag{21}$$

where

$$f(L_1, L_2, L_3, L_4) = (\sin(A_1 L_2) - \sin(A_1 L_1)) \cdot (\sin(A_2 L_4) - (\sin(A_2 L_3)), \quad (22)$$

and

$$g(M_1, M_2, M_3, M_4) = (\sin(A_3 M_2) - \sin(A_3 M_1)) \cdot (\sin(A_4 M_4) - (\sin(A_4 M_3)). \quad (23)$$

These integrals represent the total volume underneath the approximate weighting function surface limited to a box in the $(x, y)$ plane. The integral in the denominator is over all of the bottom, so it is limited by the limits imposed on the approximate weighting function. Because of the normalization, the denominator of (21) has a value of

$$R_s + R_b D(1 - R_s)^2.$$

The term in the numerator is the frequency limited part. How the frequency limits present themselves is considered in the next chapter.

It is convenient to discuss the effects of the approximate weighting function. Looking at Figure 6 on page 26, we note that the cosine has no tails, so that the weighting function equals zero everywhere outside a box on the $x$-$y$ plane. All of the volume under the surface described by the weighting function is localized around the specular point. This is not true for the Gaussian. Consequently, the Gaussian weighting function will always predict some small loss, whereas the cosine will predict exactly zero loss if the frequency limits encompass the whole box. However, in these cases, the losses predicted are less than 1dB and are negligible for this work. Also, the cosine is "fatter". For small frequency windows, the fraction of volume within the frequency window will be larger for the cosine than for the exponential. Consequently, the approximate weighting function will tend to underestimate the losses for small frequency windows. This ends up being a good tendency, as will be explained later.

## 2.5. The Limits

All that remains to get a number from equation (21) is to put limits on the area to be integrated in the numerator, ie to define $L_1 - L_4$ in terms of $x$ and $y$ given $f$ limits. This requires a knowledge of how the frequency is shifted over the bottom. It can be shown [4] that the Doppler shift at the receiver referenced to the specular point is

$$\Delta f = v_s \cos(\beta_s - \phi_1)\cos(\theta_1) + v_r \cos(\beta_r - \phi_2)\cos(\theta_2) - \Delta f_0,$$

where $v_s$ and $v_r$ are the source and receiver velocities, $\beta_s$ and $\beta_r$ are their bearings away from the specular direction, and $\Delta f_0$ is the Doppler shift at the specular point referenced to the source.

$$\Delta f_0 = \left(\frac{v_s \cos(\beta_s)}{c} + \frac{v_r \cos(\beta_r)}{c}\right) \cdot \cos(\phi_s). \tag{24}$$

It should be noted that we are dealing with fractional frequency shifts of the form $\frac{\Delta f}{f}$ here.

Using the same identities for the trigonometric functions as were used on the slope calculations, we get

$$\Delta f = \frac{v_s \cos(\beta_s)}{c}\frac{R+x}{a} - \frac{v_s \sin(\beta_s)}{c}\frac{y}{a} + \frac{v_r \cos(\beta_r)}{c}\frac{R-x}{b} - \frac{v_r \sin(\beta_r)}{c}\frac{y}{b} - \Delta f_0.$$

If we now take the case of a stationary receiver and the source approaching directly ($\beta_s = 0, v_r = 0$) then the above equation simplifies to

$$\Delta f = \frac{v_s}{c_w}\frac{R+x}{a} - \Delta f_0 = \frac{v_s}{c_w}\frac{R+x}{\sqrt{(R+x)^2 + y^2 + h^2}} - \Delta f_0 \tag{25}$$

If we are given the frequency limitation of the processor used, we can set the absolute $\Delta f$ to a constant in the above equation, and solve for a curve on the $(x, y)$ plane. Since the receiver is assumed to have a symmetric band of frequencies that it will detect, we can do the same for the negative Doppler

shift, and get a second curve. It is the area between these two curves that the receiver picks up sound from. All other points on the bottom reflect sound that is Doppler shifted outside the processor's frequency band. Finding and plotting the $x$-$y$ curve resulting from the equation above, we get the following $x$-$y$ relation, which is then plotted for a frequency window of $\pm 0.0001$ (relative Doppler shift) on Figure 7 (p. 27).

$$(R+x)^2(1-P)-y^2=(Ph)^2, \qquad P=\frac{c(\Delta f+\Delta f_0)}{v_s}.$$

As you can see in Figure 7, and as is apparent from the equation, the area to be integrated over is the intersection of two hyperbolas. We want to integrate over the bottom when the areas are bounded by straight lines. So we will again make an approximation that the area detected over the bottom is a box.

Setting $x=0$ in equation (25) we get

$$y=\pm\sqrt{(R/P)^2-R^2-h^2}, \tag{26}$$

which we will use as the $y$ limits of our box. Setting $y=0$ we get

$$x=-R\pm\frac{\sqrt{P^2+y^2+h^2}}{\sqrt{1-P^2}}. \tag{27}$$

The part pertaining to the negative sign on the square root in the $x$ term represents the part of the hyperbola mirror imaged to the other side of the source, and is a leftover of the hyperbola equation. So only the positive sign on the square root is used in determining the limits on $x$. Two limits on $x$ are obtained, one corresponding to each sign on $\Delta f$, which is buried in $P$. The limits $L_1-L_4$ and $M_1-M_4$ are computed from these relations and given in Sect. 2.6.

Note that the box is always going to be smaller than the area between the two hyperbolas. Hence, these limits will tend to overestimate the system loss. Hopefully, this tendency of the limits to overestimate the loss will offset the

projected tendency of the approximate weighting function to underestimate the loss.

Note that the frequency limited area on the bottom is symmetric about the $x$-axis (the source receiver line). We can reduce the math somewhat by calculating the partial energy for positive $y$ only, and multiplying by two. Thus, $f$ and $g$ lose one argument apiece.

$$f(L_1, L_2, L_3) = 2\int_{L_1}^{L_2}\int_{0}^{L_3} \cos(A_1 x)\cos(A_2 y)dxdy,$$
$$= 2\sin(A_2 L_3)(\sin(A_1 L_2) - \sin(A_1 L_1)) \qquad (28),$$

and similarly

$$g(M_1, M_2, M_3) = 2\sin(A_4 M_3)(\sin(A_3 M_2) - \sin(A_3 M_1)). \qquad (29)$$

In this study, for simplicity, we have defined the frequency restricted area as being approximately a box. However, these weighting functions can be integrated in a closed form for areas generated by arbitrary lines. One can see that by putting together line segments, very complex areas of the bottom could possibly be delineated, and much closer approximations to the true area be made.

## 2.6. The Final Solution

Gathering all of the above math into one statement, equation 30, the frequency loss of a system with a window of $2\Delta f$ is approximated by

$$L_s = \frac{R_s f(L_1, L_2, L_3) + R_b(1 - R_s)^2 D g(M_1, M_2, M_3)}{R_s + R_b D(1 - R_s)^2}, \qquad (30)$$

where

$$f(L_1, L_2, L_3) = 2\sin(A_2 L_3)(\sin(A_1 L_2) - \sin(A_1 L_1)),$$

$$g(M_1, M_2, M_3) = 2\sin(A_4 M_3)(\sin(A_3 M_2) - \sin(A_3 M_1)),$$

$$A_1 = \frac{h\arccos(1/e)}{\sigma_s(h^2+R^2)}, \qquad A_3 = \frac{S_{xb}|_{x=R}\arccos(1/e)}{R\sigma_b},$$

$$S_{xb}\,|_{x=R} = \frac{R}{h_a}\frac{\sqrt{4R^2+h_a^2}-h_a}{\sqrt{4R^2+h_a^2}+h_a} + \frac{R}{h_a},$$

$$R = \frac{h}{\tan(\theta_s)}, \qquad h_a \approx \frac{c_w}{c_s}h + s,$$

$$A_2 = \frac{\arccos(1/e)}{h\sigma_s}, \qquad A_4 = \frac{\arccos(1/e)}{h_a\sigma_b},$$

$$R_s = \left(\frac{\rho_s c_s \sin(\theta_s) - \rho_w c_w \sin(\theta_b)}{\rho_s c_s \sin(\theta_s) + \rho_w c_w \sin(\theta_b)}\right)^2$$

$$L_1 = \max\left(\frac{-\pi}{2A_1}, -R + \sqrt{\frac{h^2}{(\cos(\theta_s) + c_w\Delta f/v_s)^2} - 1}\right),$$

$$L_2 = \min\left(\frac{\pi}{2A_1}, -R + \sqrt{\frac{h^2}{(\cos(\theta_s) - c_w\Delta f/v_s)^2} - 1}\right),$$

$$L_3 = \min\left(\frac{\pi}{2A_2}, \sqrt{(\frac{R}{c_w\Delta f/v_s - \cos(\theta_s)})^2 + R^2 + h^2}\right),$$

$$M_1 = \max\left(\frac{-\pi}{2A_3}, -R + \sqrt{\frac{h_a^2}{(\cos(\theta_b) + c_s\Delta f/v_s)^2} - 1}\right),$$

$$M_2 = \min\left(\frac{\pi}{2A_3}, -R + \sqrt{\frac{h_a^2}{(\cos(\theta_b) - c_s\Delta f/v_s)^2} - 1}\right),$$

$$M_3 = \min\left(\frac{\pi}{2A_4}, \sqrt{(\frac{R}{c_s\Delta f/v_s - \cos(\theta_b)})^2 + R^2 + h_a^2}\right).$$

Remember that the approximate weighting functions are zero outside the first hump of the cosine, so we must be careful not to integrate past that point. That is the purpose of the min's and max's in the above equations. Also, if the specular angle is below the critical angle, all the terms involved with $g$ (ie. the apparent height, M1-M6) are not needed and need not be computed.

Granted, the formulas are long and involved, but they represent a closed form approximation that can be done on any hand calculator once the environmental factors are set.

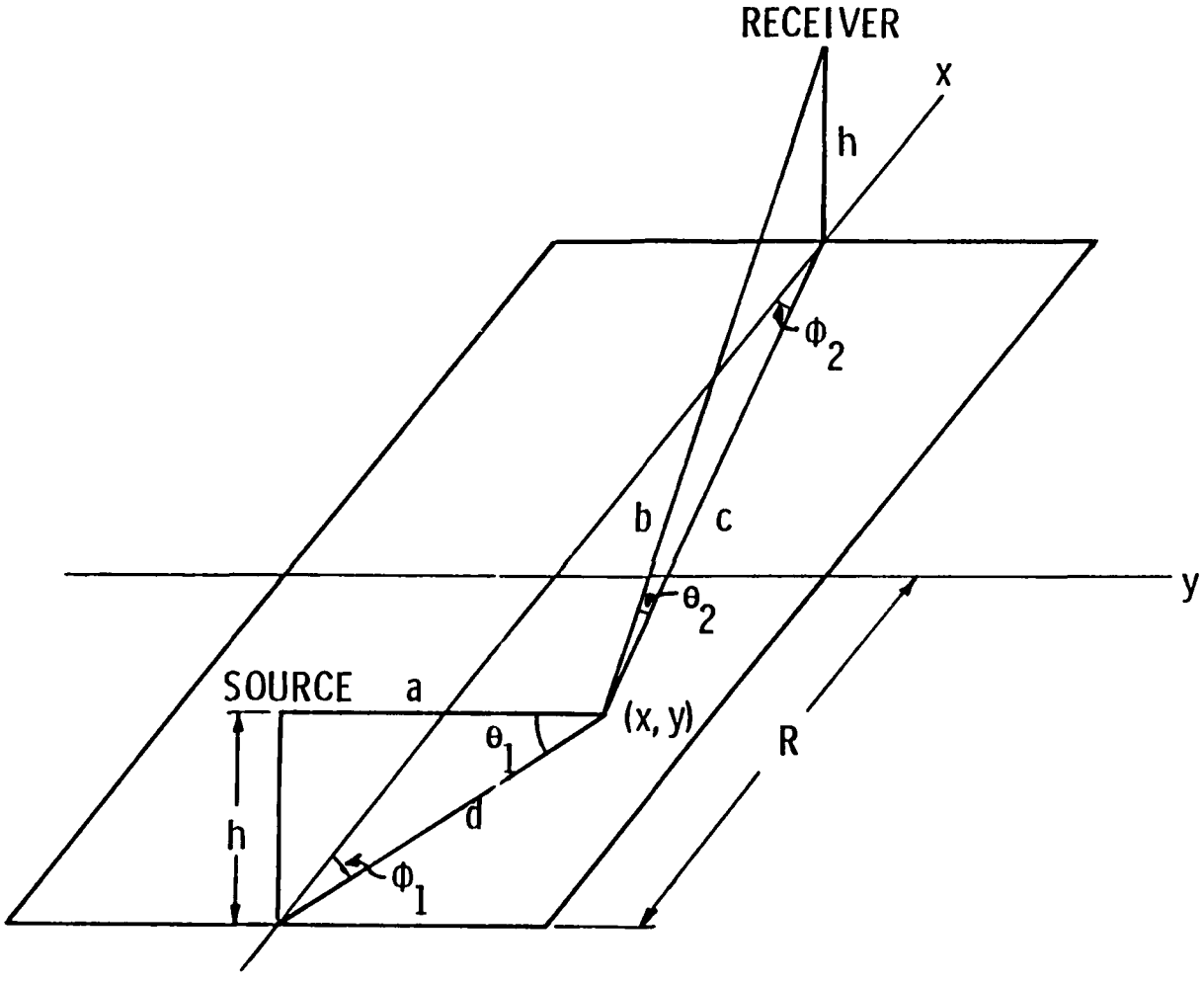


**Figure 4** Definition of Angles and Sides Used in Calculation of Bottom Slopes

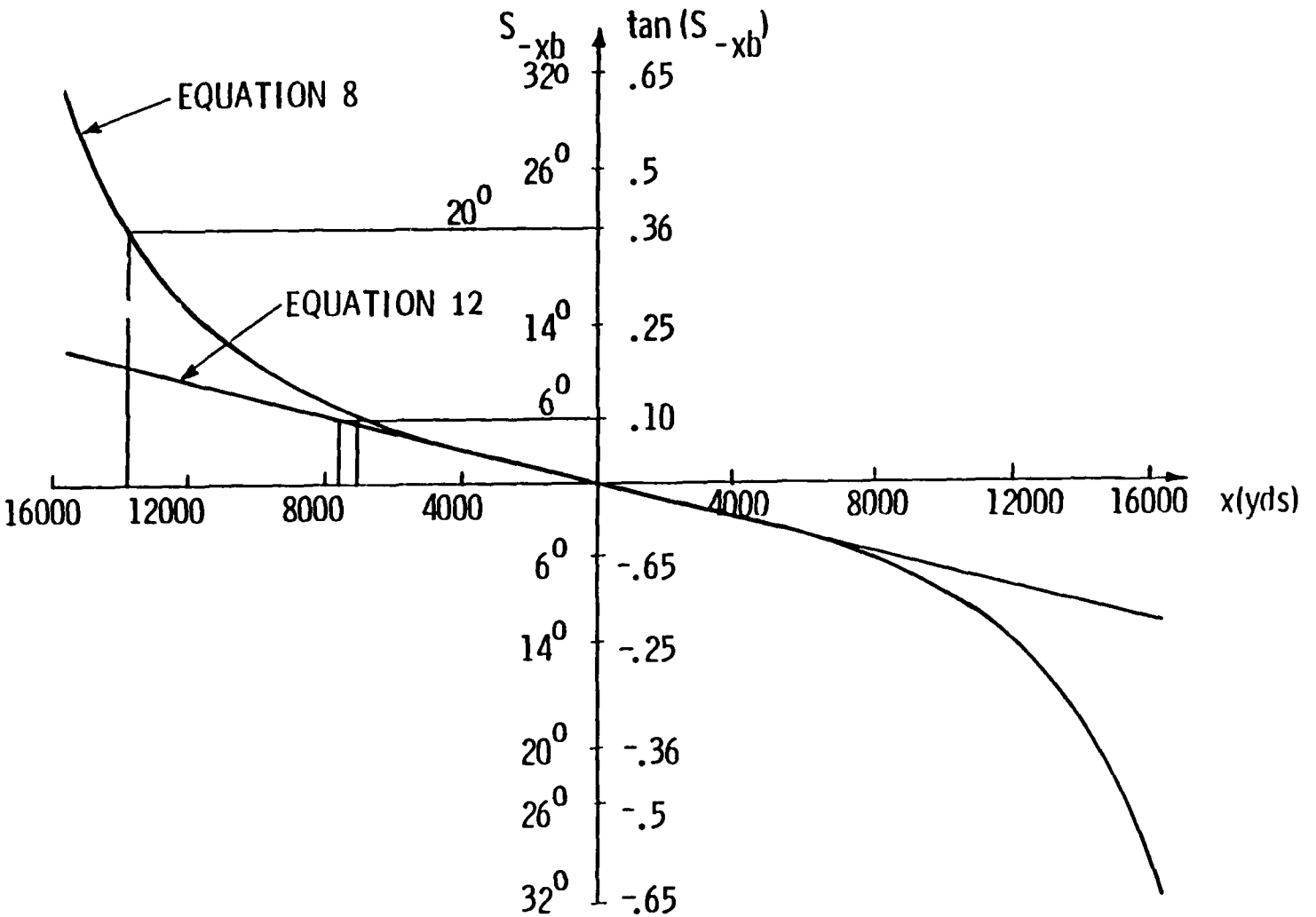


Figure 5 Comparison of Linear Approximation to Actual Computation of Sediment Slopes

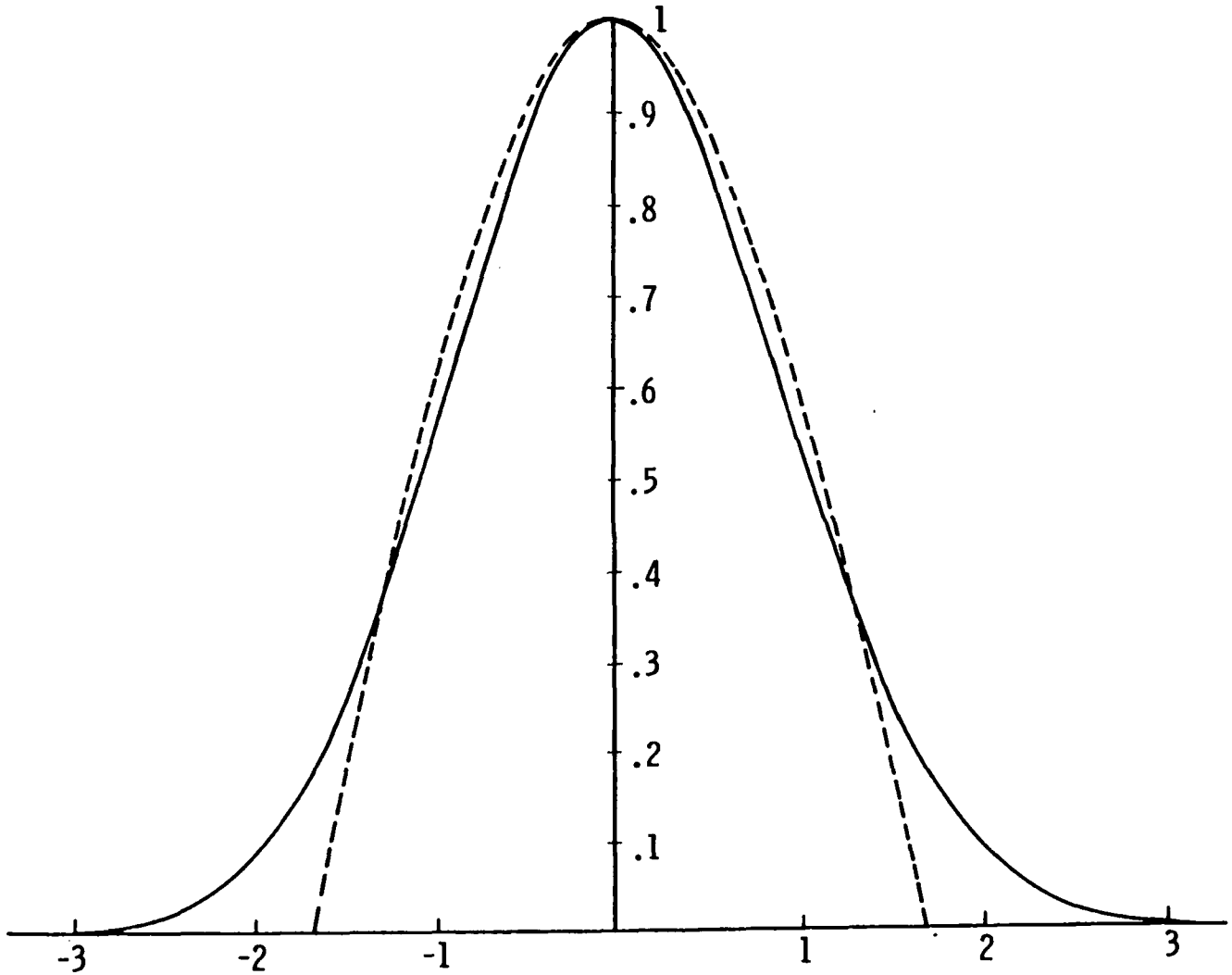


**Figure 6** Comparison of Gaussian and Cosine Weighting Functions

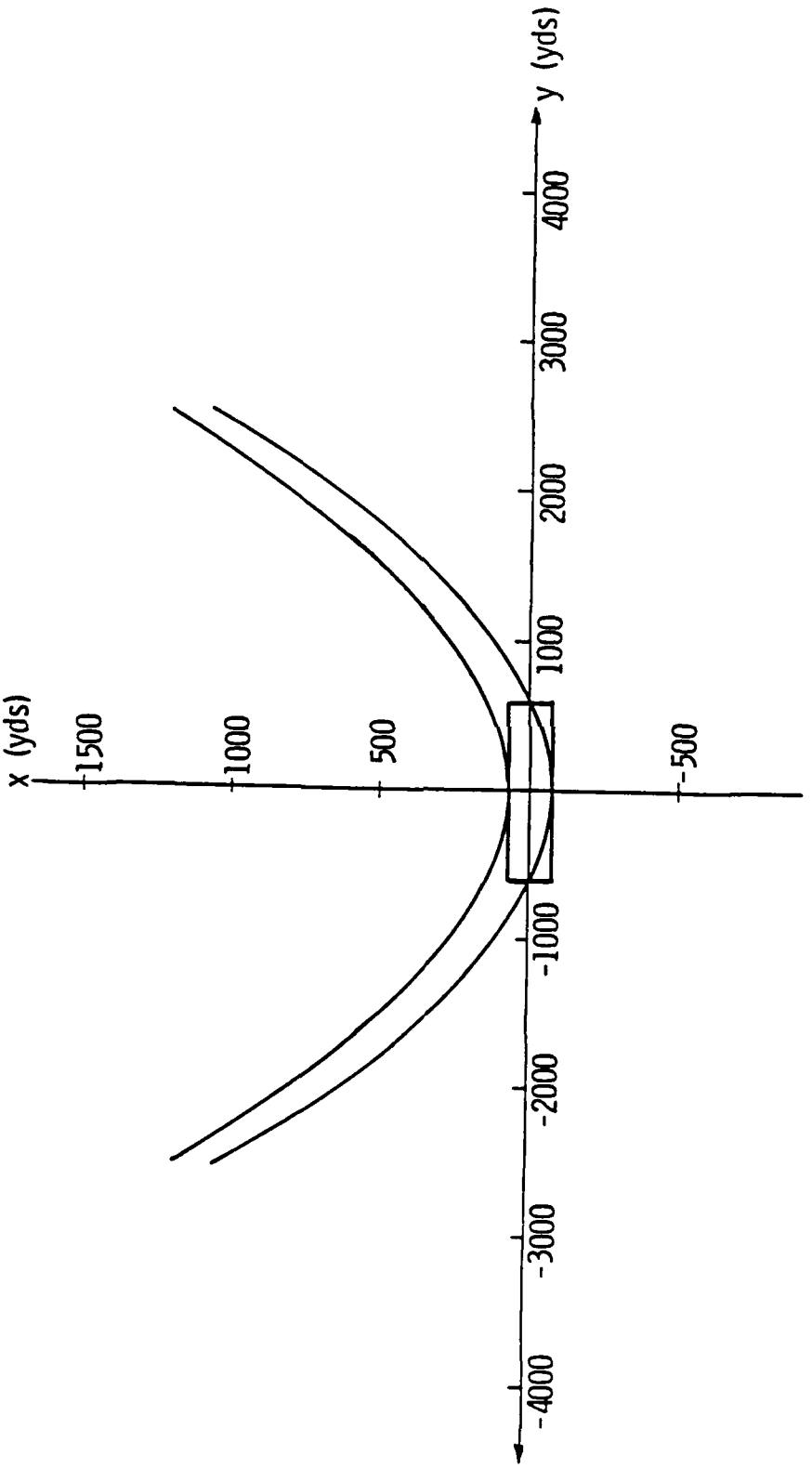


Figure 7 Frequency Limited Area on the Bottom

# Chapter 3

# THE TESTING

## 3.1. Introduction

Since this derivation is meant to reasonably accurately model a physical problem, it is necessary to test the solution. In this case we will be testing against a very involved, long, time consuming numerical model.

Equation 30 was coded into a computer along with the full model. One change was made. The apparent height was calculated exactly using the computers solution for the specular basement path. This was done to keep errors involved with the apparent height from affecting the closed form solution too badly in the some of the later tests. More study should go into the calculation of the apparent height. This is discussed later.

## 3.2. The Full Model

Now we will test all of the assumptions and formulas we have derived. To do this, we will compare the results to those of a full bottom scattering model [4]. This model uses ray tracing techniques to set up tables of range *.vs.* angle into the sediment for both the water and the sediment. It then iterates over a grid on the bottom, finding the angle into the sediment at each point by searching the ray tables for the correct range. Having done this, the program assigns a Gaussian probability to the point, calculates the reflection coefficient at the point using the actual angle into the sediment at that point, the absorption at the point (if it is doing the sediment penetrating path) and the Doppler shift at the point. It keeps a running sum of the energy coming off the bottom, and also a running sum of the energy returning for which the Doppler shift is within the range given. This model assumes a general SVP in the water column, an empirical SVP in the sediment, and will also handle a beam pattern associated with the receiver.

For these tests, the beam pattern was set equal to unity for all $(x, y)$.

The model takes as inputs sediment thickness, density, and sound speed, a water SVP, source and receiver depths, and source and receiver speeds and bearings. It assumes a rather complicated empirical formula for the SVP in the sediment which has two parameters associated with it which determine the steepness of the gradient right under the water/sediment interface and the curvature of the SVP throughout the sediment.

### 3.3. The Assumptions

First we will test the assumptions we initially made regarding the reflection coefficient and the absorption in the sediment being constant over the whole bottom. A short summary of the nature of the reflection curves is in order here.

Harking back to classical wave theory, the reflection as a function of angle of incidence is given by

$$R_s(x,y) = \left( \frac{\rho_s c_s \sin(\theta_w) - \rho_w c_w \sin(\theta_r)}{\rho_s c_s \sin(\theta_w) + \rho_w c_w \sin(\theta_r)} \right)^2$$

Three cases appear. When the speed of sound in the sediment is greater than that in the water, there exists a critical angle, below which all energy is reflected back into the water, and no energy enters the sediment. In the ocean, these critical angles generally occur between 0 and 20 degrees. When $c_w < c_s$ and $\rho_w c_w > \rho_s c_s$ or $c_w > c_s$ and $\rho_w c_w < \rho_s c_s$ an angle of intromission occurs where there is total transmission. Generally speaking, plots of reflection *.vs.* angle take on the three shapes in Figure 8, which is found on page 38. In the real ocean, case number three never occurs because of the nature of ocean sediments: they are always denser than the water above them.As can be seen, the reflection coefficient appears to stay rather constant for angles less than 10 degrees and angles greater than 40 degrees. Under 10 degrees, the reflection coefficient is low for cases of intromission angle and high for cases of critical angles. Since

it is the change of the angle of incidence at off specular points that leads to changes in reflection coefficient over the bottom, we expect the greatest variation of reflection coefficient over the bottom to occur when the specular angle falls on an area of the reflection curve where there is a lot of change, for instance if the specular angle falls near a critical angle. On the other hand, if the specular angle is up near sixty degrees, then we would expect the reflection coefficient to vary little over the bottom.

In fact this is the case. A plot of reflection coefficient $R_s$ *.vs.* $x, y$ position was made (Figure 9, p. 39) for cases with critical angles. We can see that the reflection coefficient does not change noticeably except in the one case where the critical angle is close to the specular angle. In this case, there is a great change of reflection coefficient over the bottom. However, in the end, this violation of our assumption does not hurt us as the frequency losses at these low angles are so small that they can be assumed to be zero.

Similar plots were made of total dissipation $D$ in the sediment *.vs.* $x, y$ position (Figure 10, p. 40). While there is some variation, about 10 percent, we do not believe that it is significant because, by using the absorption at the specular, the variation gets worse as we get further away from the specular point. But far from the specular point, the weighting function is falling off rapidly, so the errors in the absorption approximation are reduced from being weighted less.

### 3.4. The Slopes

Next the full formulas for the slopes as a function of $x$ and $y$ were checked (equations (7) and (8)). This was done in both the sediment and the basement to allow an evaluation of our apparent height approximation. In Figure 11 on page 41, the $x$-$z$ slope is plotted over $x$ and $y$. The top surface is the models' iterative solution, and the bottom is equation 8. The $x$ and $y$ scales are chosen to get

full coverage by the weighting function, and the exact scales are not important except that they are the same for the two plots. It is obvious in Figure 11, which applies to the sediment, that equation 8 is giving an accurate x-slope calculation. Figure 12 on page 42 shows the same calculation for the basement, but only the positive $x$ axis is plotted. In all these plots, $y$ was set equal to zero in the calculated slope but not in the full model slope in order to get a grasp on how badly the assumption that $S_x$ is independent of $y$ hurts. Because of the increased roughness of the basement, the plot goes out much further in $x$ and $y$, and the $x$ slope shows some dependence on $y$ in these plots. However, equation 8 with $h$ replaced by $h_a$ is still very accurate. This instills confidence in the use of the apparent height to account for refraction in the sediment.

The equation for the $y$ slope was exact, and no testing had to be done for it. During debugging, some plots of $y$ slope were made, and the calculation is correct.

As shown in Figure 5 (25), the linear approximation for $x$-slope on the sediment, equation 12 is a good one due to the small rms roughness of the sediment. No further testing of the linear approximation of $S_x$ was done.

In the basement, the linear approximation to the $x$-slope is not as good, as is illustrated in Figure 13 (p. 43). For simplicity, the slope is shown only for $y = 0$, on the source receiver line. The error is not large and, as will be seen next, the weighting functions have the right shape.

### 3.5. The Weighting Function

Having now verified our slope approximations, we will see about our cosine weighting function. The approximate weighting function, equation (19), over the bottom for the sediment gives the surface of Figure 14 (p. 44), and the real weighting function is also given. We can see that, though obviously the two

surfaces are not identical, they do have the same shapes, and most importantly, they fall off at the same point. Similar surfaces were plotted for other specular angles, and the agreement was as good.

Exactly the same surfaces were examined for the basement. These surfaces were very similar to those in Figure 14. Again, though the cosine weighting functions were obviously different from the Gaussian functions, the cosine functions had a similar shape and they fell off at approximately the right point.

As a final check of the kernel of the integral, the full model was run for each environment and two loss numbers were generated. The results are tabulated and plotted in Figure 15 on page 45. The "Full Model" loss is the loss the full model calculates. The "Approximate" loss is the loss calculated using the cosine weighting functions, the constant reflection coefficient, and the constant absorption coefficient. However, the frequency limits are not those given by equations 26 and 27 but were selected in the exact same manner as the full model. In other words, the "Approximate" loss is exactly the same as the "Real" loss except that the new quantities for the weighting function W have been inserted. The top curves are for a thin sediment (40 yards), while the bottom curves are for a thicker sediment (800 yards). We can see good agreement everywhere, which instills confidence in the approximations we have tested so far. It should be noted that these losses were calculated for a $\Delta f$ of 0.0001, which is very low. This was done so that larger losses would be obtained, and errors thus magnified. In practice, frequency windows smaller than 0.0005 are rare, since that corresponds to a filter $Q$ of 2000.

### 3.6. The Limits

Having now gained some confidence in the weighting function to be used, we will check the limits, and thus the final answer.

Contour plots were made showing the areas both inside the hyperbolas and inside the boxes of equations 26 and 27. They were very similar in appearance to Figure 7 (p. 27). As is to be expected, the area inside the box is always smaller than the area between the hyperbolas, which would manifest itself as an over-approximation of the loss. However, the approximate weighting functions tend to under-estimate the loss, so some of the errors tend to cancel themselves out.

### 3.7. Regions of Accuracy

Looking at Figure 16 on page 46, we see the losses calculated from equation 30. compared to those of the full model. Here, a height of 5000 yards and a $\Delta f$ of 0.0001 were used. A plot of the errors is also given in Figure 16. You can see that the numbers generated by equation 30 are generally within 1.5 dB, which is good for such an approximate solution. It was apparent from other similar runs that the approximate, closed form solution is doing a good job of estimating the frequency loss in all types of environments where the assumptions made are not violated (isovelocity profiles, same source and receiver depths, etc).

An attempt to devine an understanding of the sources of the the errors in figure 16 will now be made. For low angles, the errors inherent in the approximate weighting functions appear to dominate. At these low angles, the weighting functions on the bottom become very elongated in the $x$ direction, almost like a tunnel. We can some effect of this in figure 14 (p. 44), which was made for a specular angle of 40°. Also, looking at equation 9, we cn see that $A_s$ is becoming very mall, as at these low specular angles, the range $R$ is very large. Scince the approximate weighting function goes as $\cos(A_1 x)$ and $A_1$ is proportional to $A_s$, which is small, x must get very large before the weighting function drops off. Also, most of the frequency limiting goes on in the $x$ direction. That is, the

tunnel is truncated in the lengthwise direction, but not in the width direction. The approximate weighting function does not fall off in the $x$ direction as fast as the gaussian weighting function, so the loss is under-estimated. As the angle increases, the weighting functions begin to match a little better, and now the errors made in the frequency approximations begin to dominate the errors. The errors increase at higher angles mostly because the total loss increases. As a fraction of the total loss, the errors stay fairly constant.

Now, one by one we will violate the assumptions made in the beginning of the derivations, to check what sort of errors they introduce when compared to real world situations.

First, we will introduce a water sound velocity profile into the full model. A reasonable one was chosen (one which happens to be 5000 yards deep to correspond to the runs we made before) , and the points and plot of the profile are shown in Figure 17 on page 47. When run with a frequency window of 0.0001 and no gradient in the sediment, as before, and the source and receiver both at 67 yards, we get the values and errors in Figure 18 (p. 48). The introduction of the SVP doesn't appear to have adversely affected the errors, and a marked similarity between Figure 16 and 18 is noted. This is because instead of using the real range between source and receiver, the closed form solution generates an apparent range, similar to the apparent height. If you will remember, the range was calculated as $h/\tan(\theta_s)$. Now with a SVP introduced, this is not the true range, but a range extrapolated from the specular angle, as shown in Figure 19 (p. 49). This range is used in calculating the slopes and in the limits, and compensates for the the refraction in the water in much the same way that the apparent height compensates for the refraction into the sediment. Thus, for the most part, the weighting function is still as correct as before. So the introduction of a water SVP does not affect the accuracy of the approximation too badly.

For the same reason the introduction of a velocity gradient into the sediment does not hurt us too badly, as long as the sound velocity at the bottom of the sedimentary layer is used to calculate the apparent height, which will take into account refraction in the sediment, and the reflection coefficient, which will keep the sound from refracting before it hits the basement. If the sound refracts before it hits the basement, then the reflection coefficient will be one if the sound speed at the bottom of the sediment is used to calculate the reflection coefficient. In other words, if the sound refracts before it hits the basement at the specular point, it will appear to the basement as if the specular angle is below the critical angle. An illustration of the apparent range is given in Figure 19 on page 49. The errors resulting from adding the sediment SVP are shown in Figure 20 on page 50. Although the full model uses a complicated function of sound velocity with depth, for the high initial gradients chosen for this test, the gradient in the sediment is essentially constant. Again, the effect was not detrimental when compared to the already existing errors. Note also that, because the SVP in the sediment is always positive, the travel path in the sediment will be longer, which should decrease the loss a bit and perhaps increase the accuracy of the closed form solution by decreasing the importance of the basement path.

Also note how the errors are tending more towards over-estimation, even for the lower specular angles. This is due to critical angle limiting, which the closed form solution ignores. At the specular point, the angle into the sediment is above the critical angle. However, as we move out in $x$ towards the receiver, there is a point where the sound entering the sediment is below the critical angle, and no reflection off the rougher basement can occur. Thus, no energy is returned from these far off-specular points in the real case. However, we have ignored the variation in the reflection coefficient in the derivation of the closed form solution. Thus, as far as the simplified equation can tell, there is energy returning from

those far off-specular points. Thus too high a loss is reported.

Introduction of a sediment sound speed gradient creates another problem: the calculation of the apparent height can no longer be done with the simple equation of Appendix C because the sound speed ratio between the water at the water/sediment interface and the bottom of the sediment will be significantly different than one now. That is why the "real" apparent height generated by the full model is used in this study. It was necessary to separate errors caused by the weighting functions and estimated limits and the errors caused simply by the apparent height being wrong. The errors in apparent height can make very large errors in the estimated loss. So while the equations in Appendix C are good for thin sediments where the highest losses occur, they are not used here. However, the full model is not needed to get a good estimation for the apparent height. A simple program to solve the transcendental equation will do the job sufficiently accurately. It should be noted that the errors given in Figure 20 also include the water SVP as well.

We will now offset the source and receiver depths. We expected this to have the worst effect of the three assumption violations. Shifting the relative positions of the source and receiver skews the weighting function on the bottom from front to back, especially in shallow water. The approximate weighting functions will no longer resemble the true weighting functions by any stretch of the imagination. I expected this to severely hurt the closed form approximation

The depth of the receiver was used as $h$ in the equations, as it was felt that the receiver depth was more likely to be known. Figure 21 on page 22 shows the errors and values obtained by running with the same water and sediment SVP as table 4, but now the source is 33 yards deep and the receiver at 200 yards. We see some increase in the errors, but still they remain below 2 dB. We believe that the reason is because a change of 167 yards between source and receiver depth

is insignificant in 5000 yards of water.

Lastly, as a worse case test, a shallow water profile (1800 yards as opposed to 5000 yards) with a strong surface duct, the receiver and source displaced across the duct (at 6 and 100 yards respectively) and a steep gradient in the sediment was run and compared to this simple model. Again the receiver depth was used as $h$, and the sound velocity at the bottom was used as $c_w$ and the sound velocity at the bottom of the sediment used as $c_s$. Errors do occur, as shown in Figure 22 (p. 52), but still within 2 dB. For such a grossly overstretched model, the agreement is quite acceptable, although not entirely unexpected. We have seen that most of the approximations are taken care of by the closed form derivation. Only the lack of error caused by the shifting of the source and receiver is unexplained. I currently believe that, at low angles, the weighting function is so tunnel like that skewing it front to back makes little difference, and that at high angles, the frequency limiting is taking such a small part of the weighting function that again the skewing is not seen.

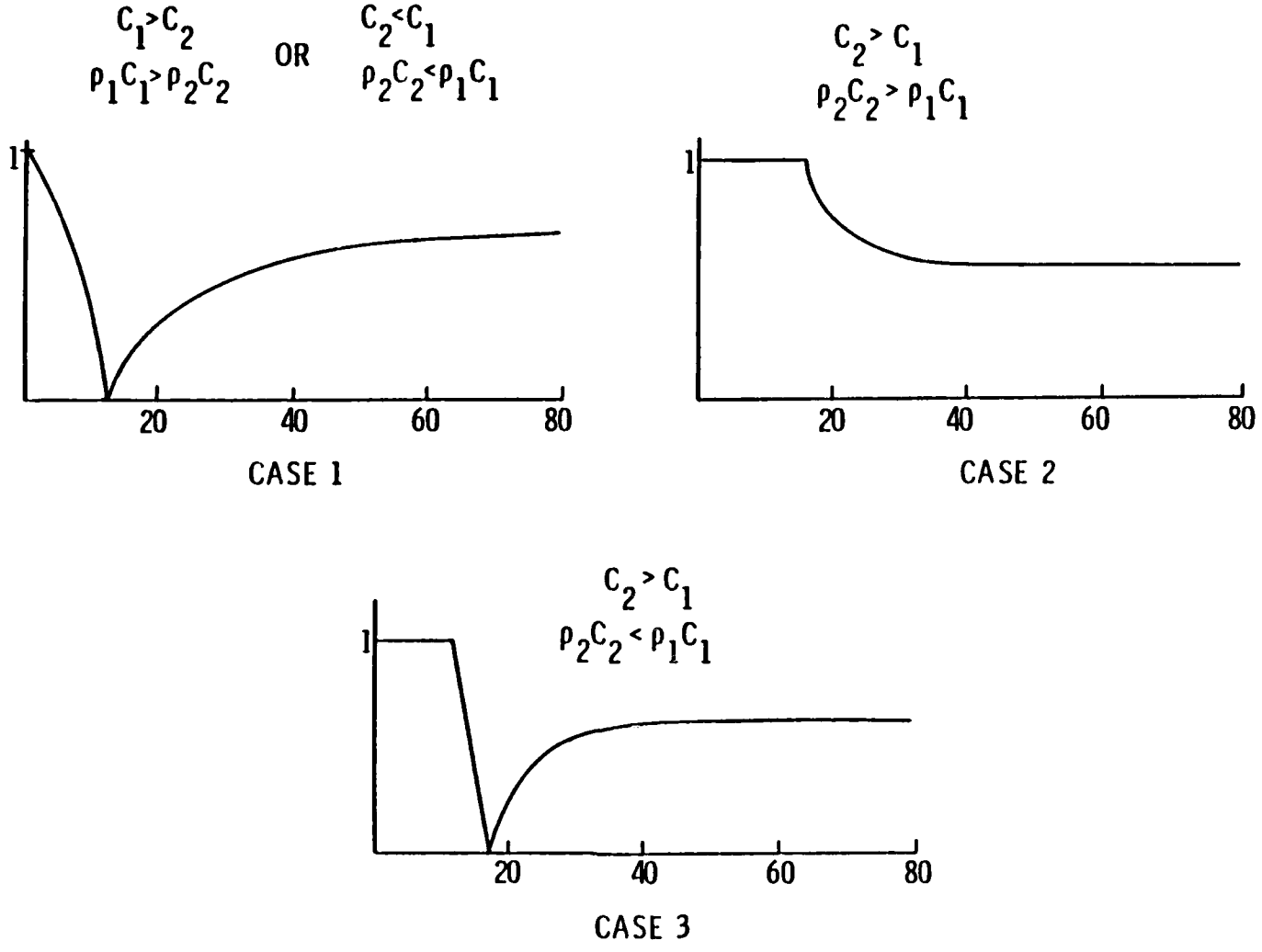


**Figure 8** **Examples of Reflection Coefficient Curves**

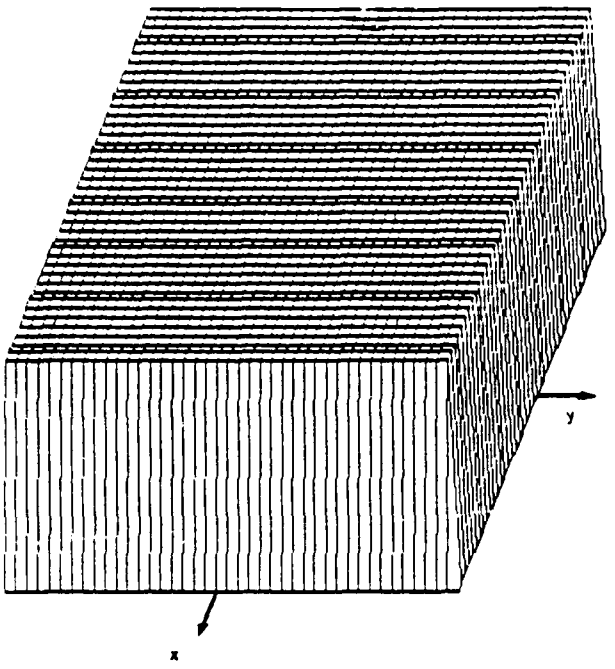


Critical Angle at 15°
Specular Angle of 60°

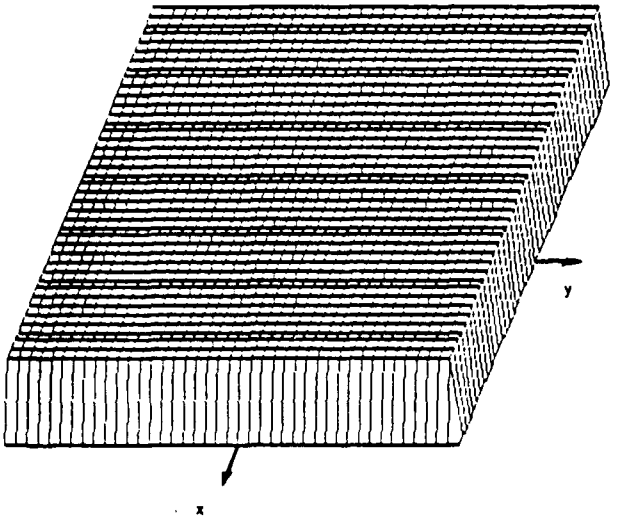


Critical Angle at 15°
Specular Angle of 20°

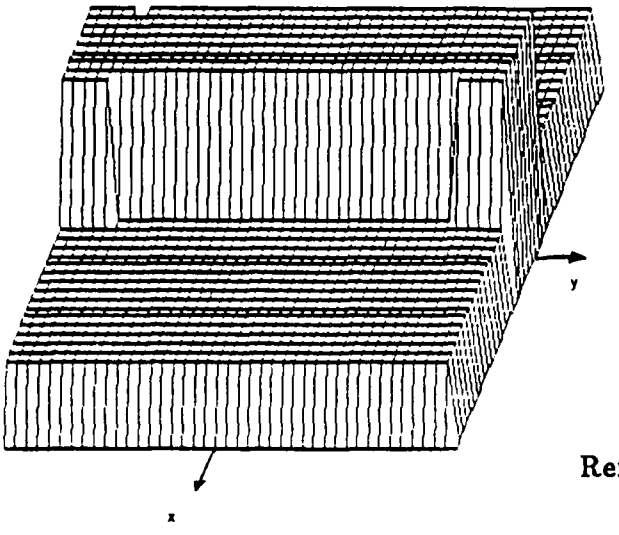


Critical Angle at 15°
Specular Angle of 16°

Figure 9

Reflection Coefficient over the Bottom

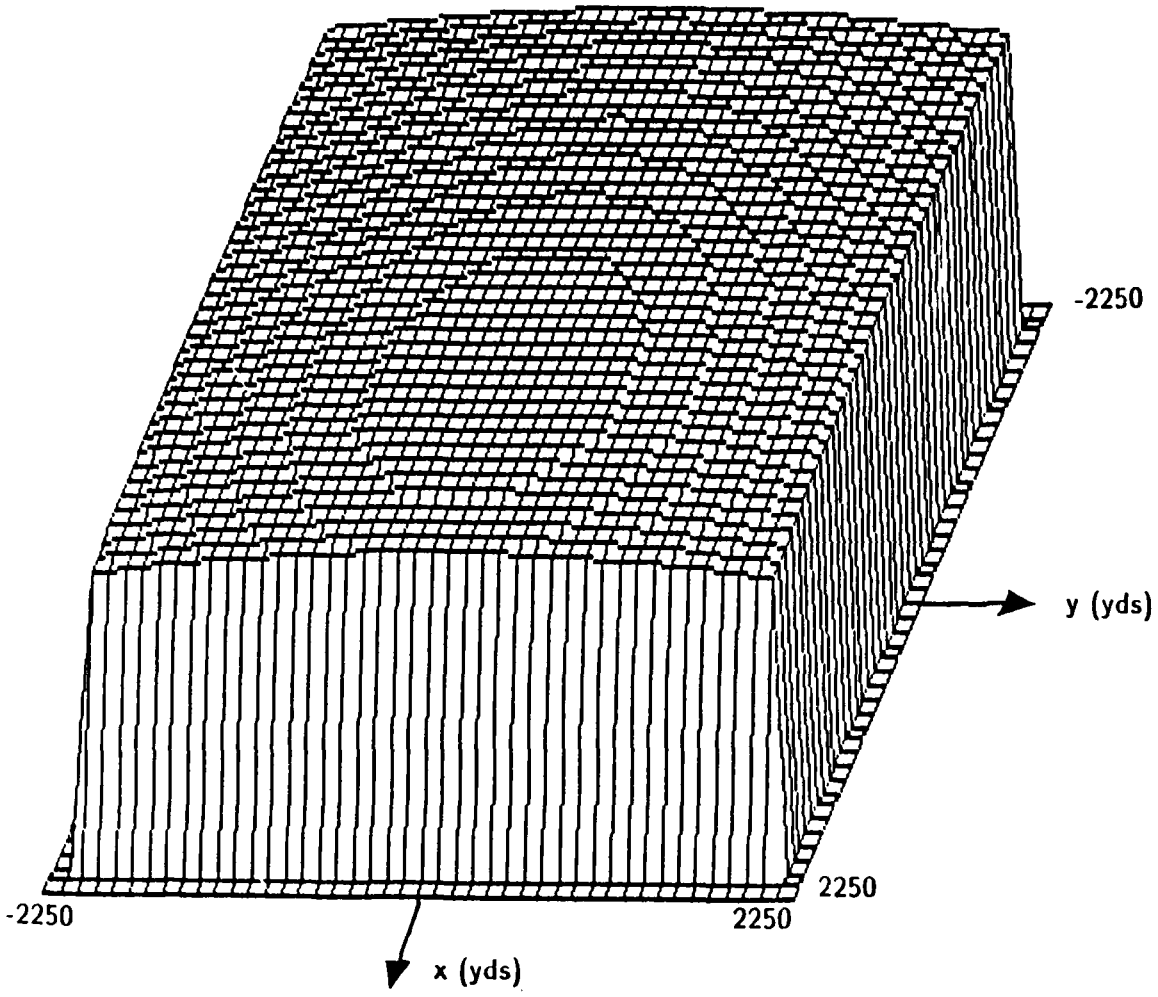


Figure 10 Absorption through the Sediment

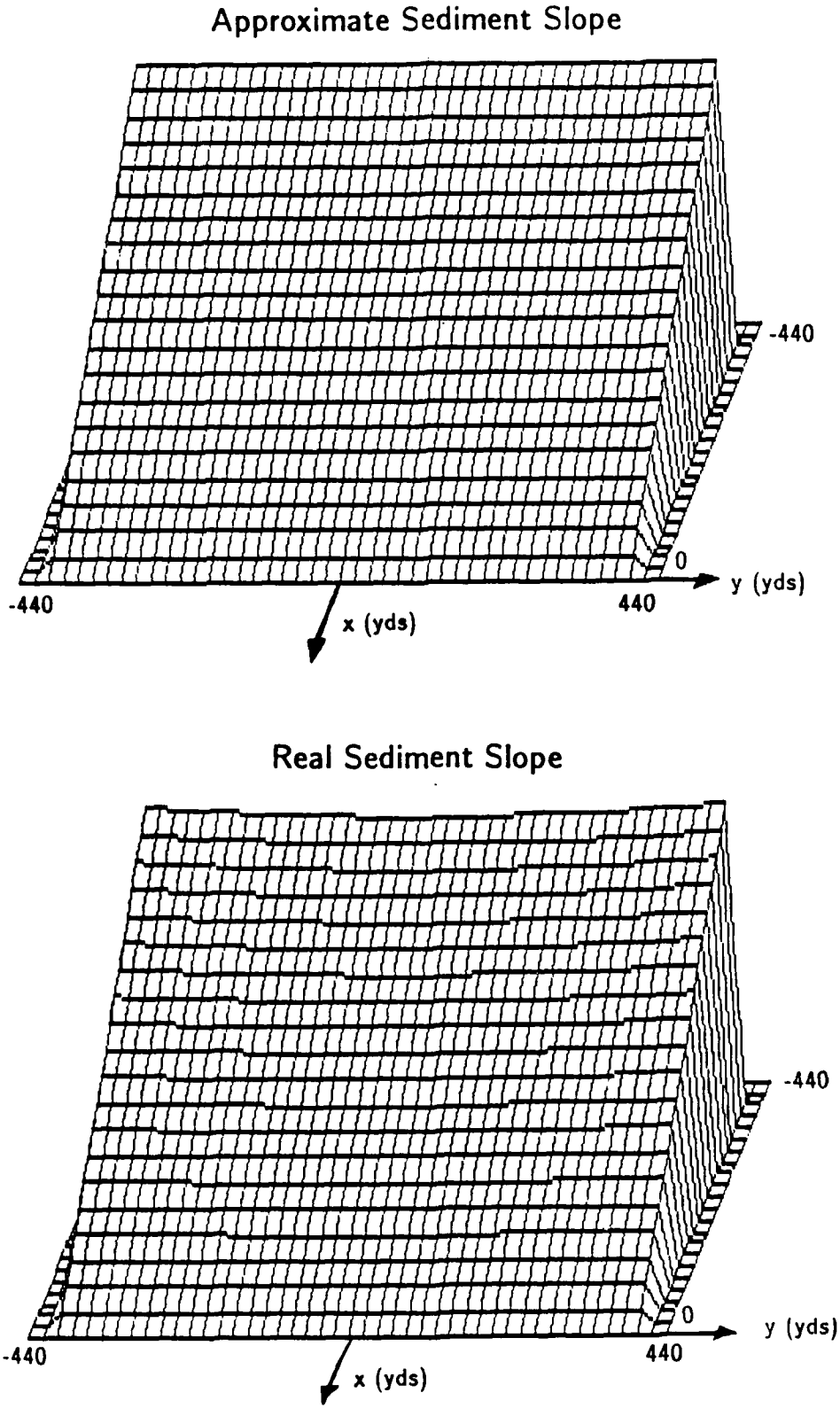


Figure 11 X-Slope over the Bottom for the Sediment

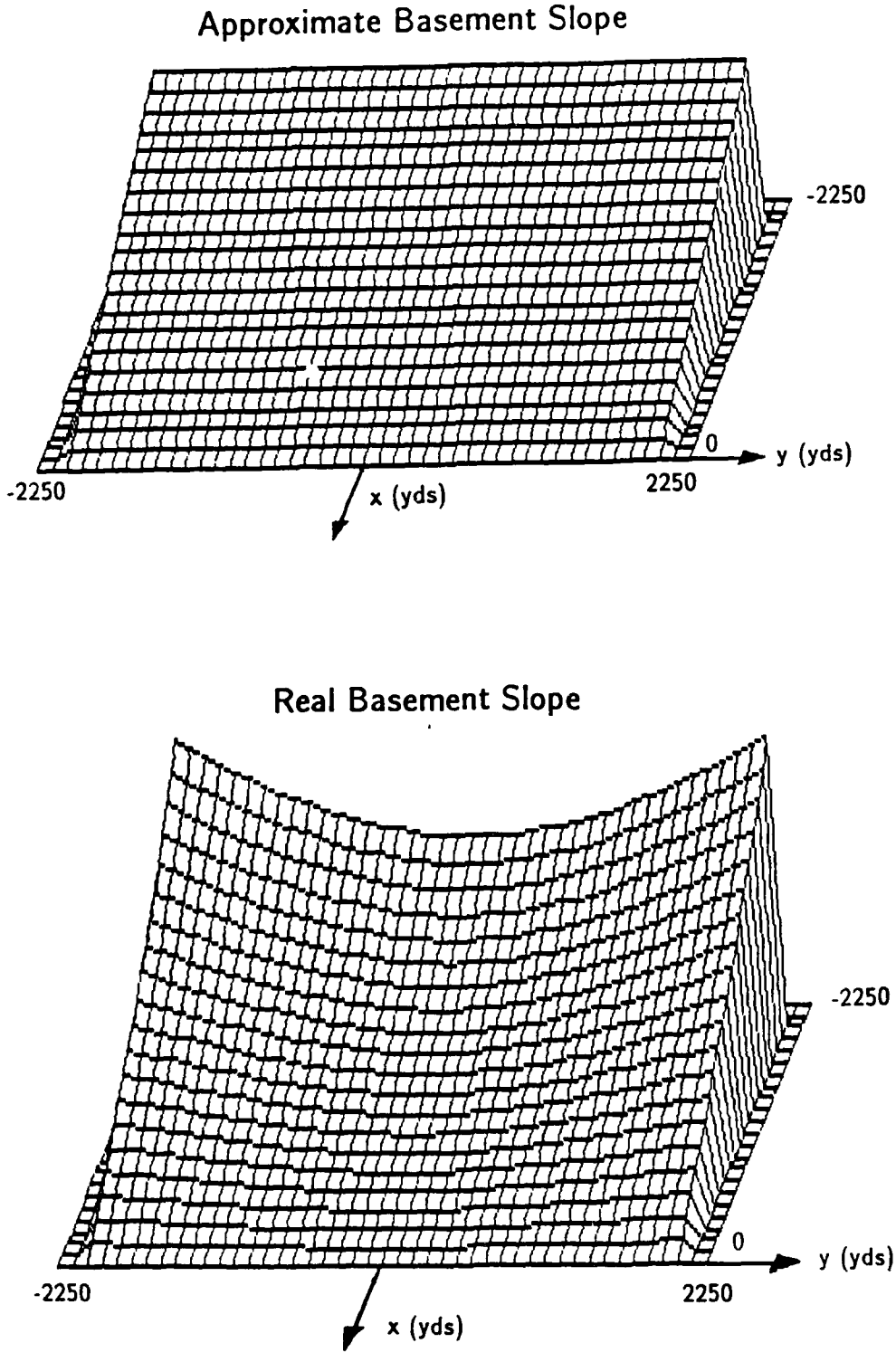


Figure 12 X-Slope over the Bottom for the Basement

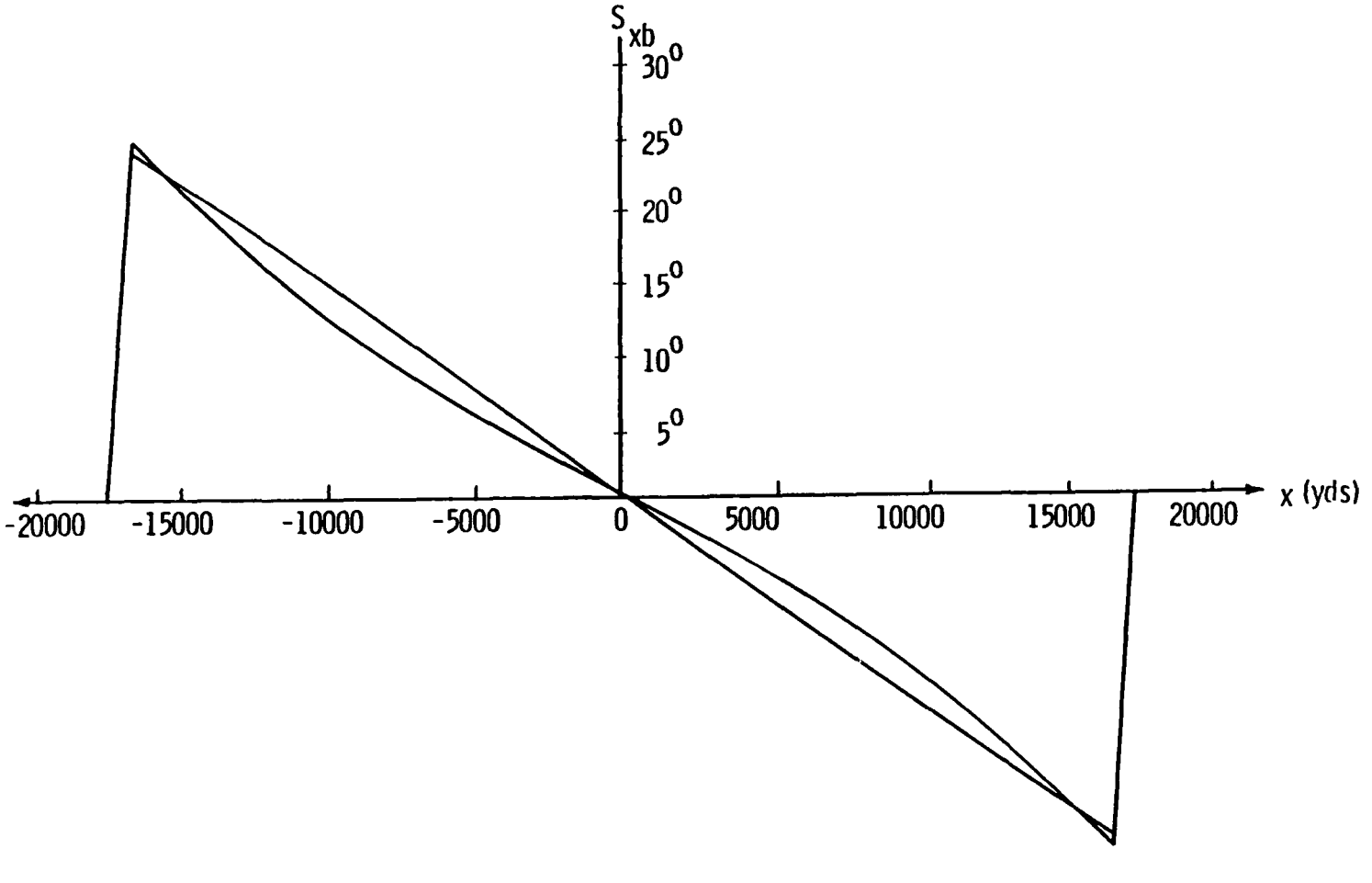


**Figure 13** X-Slope Approximation for the Basement

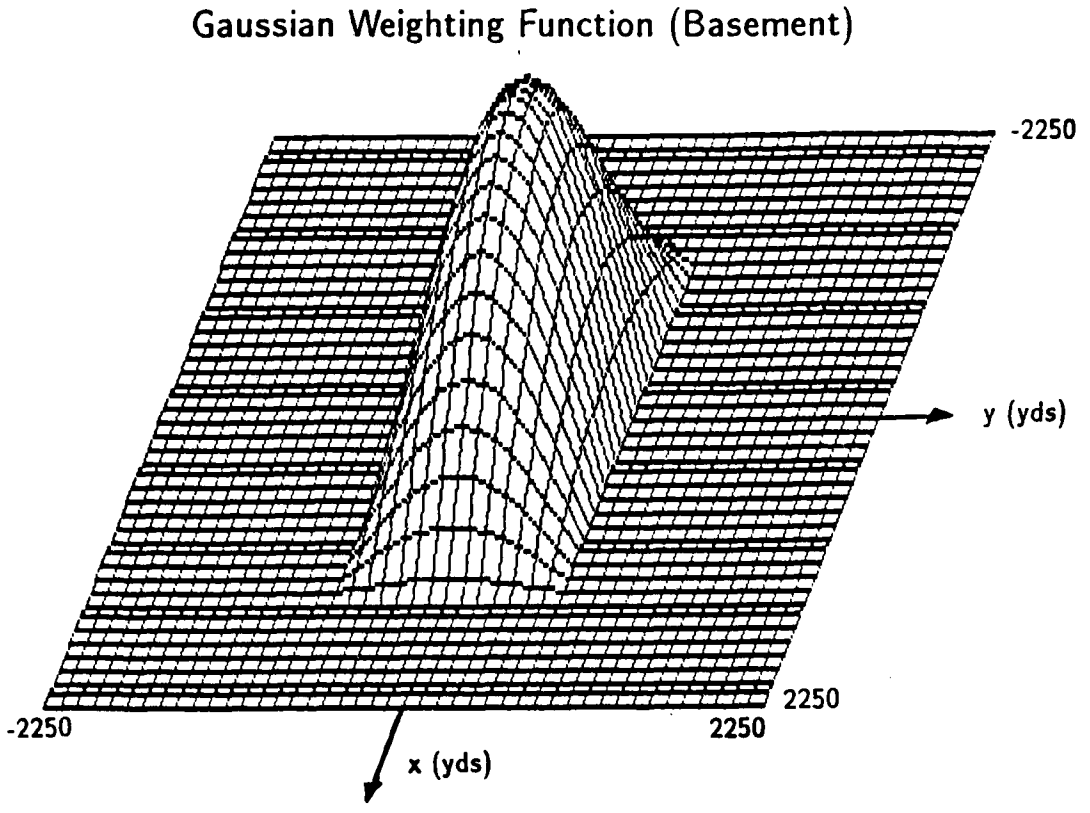


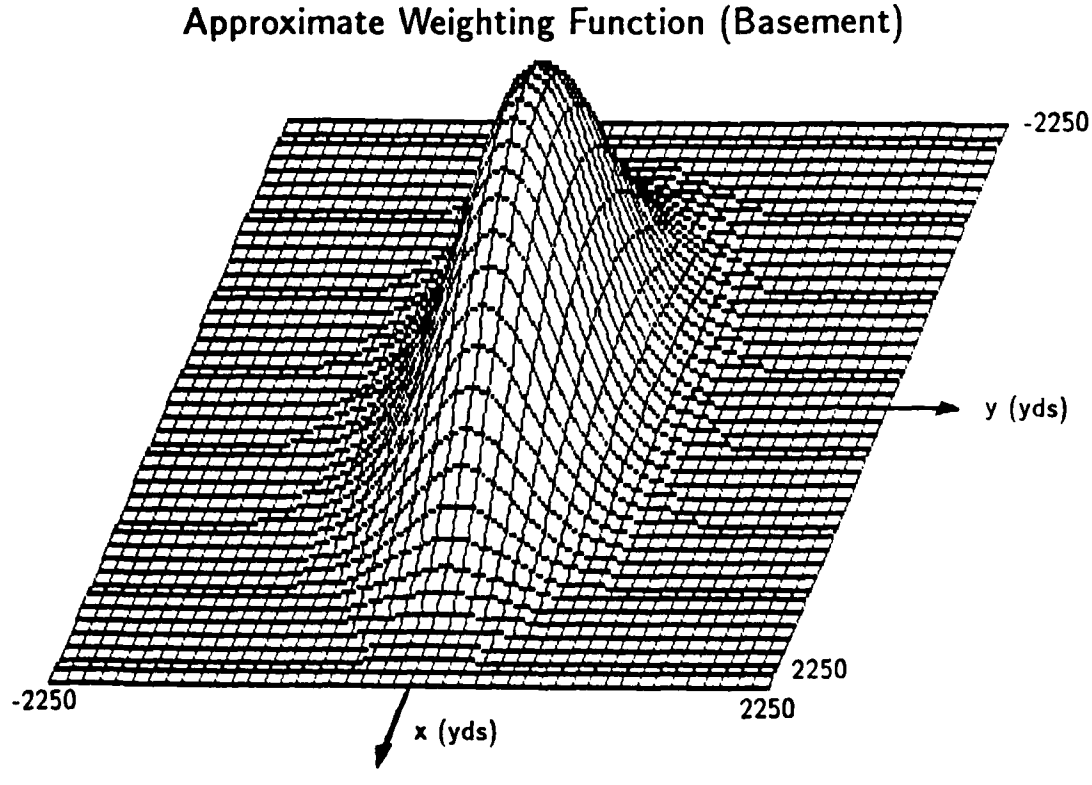


Figure 14 Weighting Function over the Basement

| Thick Sediment | | | Thin Sediment | | |
|---|---|---|---|---|---|
| Angle | Full Model | Approx | Angle | Full Model | Approx |
| 10 | 0.000 | 0.0000 | 10 | 0.0000 | 0.0000 |
| 20 | 1.5433 | 1.3726 | 20 | 3.0594 | 4.3718 |
| 30 | 3.2033 | 3.1334 | 30 | 7.0491 | 7.5295 |
| 40 | 4.2231 | 4.1195 | 40 | 8.8706 | 9.2774 |
| 50 | 6.2583 | 6.0740 | 50 | 10.7007 | 10.8219 |
| 60 | 7.4048 | 7.2397 | 60 | 11.5946 | 11.6714 |
| 70 | 8.3838 | 8.2024 | 70 | 12.4078 | 12.5192 |
| 80 | 8.6003 | 8.3725 | 80 | 11.7977 | 11.5474 |

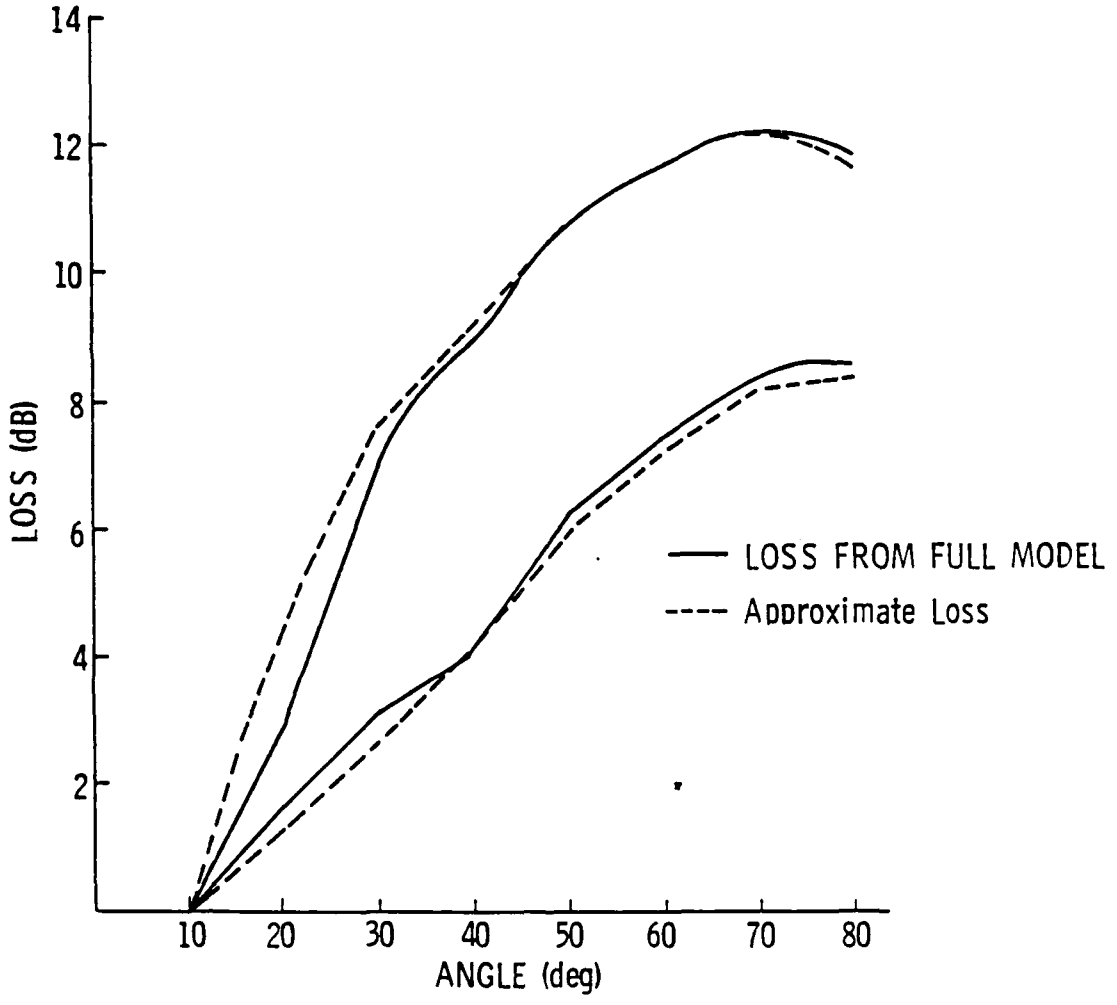


**Figure 15** **Test of the Approximate Integral Kernel**

| THICK SEDIMENT (400 YDS) | | | THIN SEDIMENT (40 YDS) | | |
|---|---|---|---|---|---|
| Angle | Full Model | Closed Form | Angle | Full Model | Closed Form |
| 10 | 0.0000 | 0.0000 | 10 | 0.0000 | 0.0000 |
| 20 | 1.5433 | 1.2205 | 20 | 3.0594 | 2.2044 |
| 30 | 3.2033 | 3.0348 | 30 | 7.0491 | 7.5709 |
| 40 | 4.2231 | 4.1700 | 40 | 8.8706 | 9.7696 |
| 50 | 6.2583 | 6.6207 | 50 | 10.7007 | 12.1022 |
| 60 | 7.4048 | 7.1788 | 60 | 11.5946 | 12.8310 |
| 70 | 8.3838 | 7.5390 | 70 | 12.4078 | 13.1379 |
| 80 | 8.6003 | 7.7259 | 80 | 11.7877 | 13.0049 |

FREQUENCY LOSS (dB)

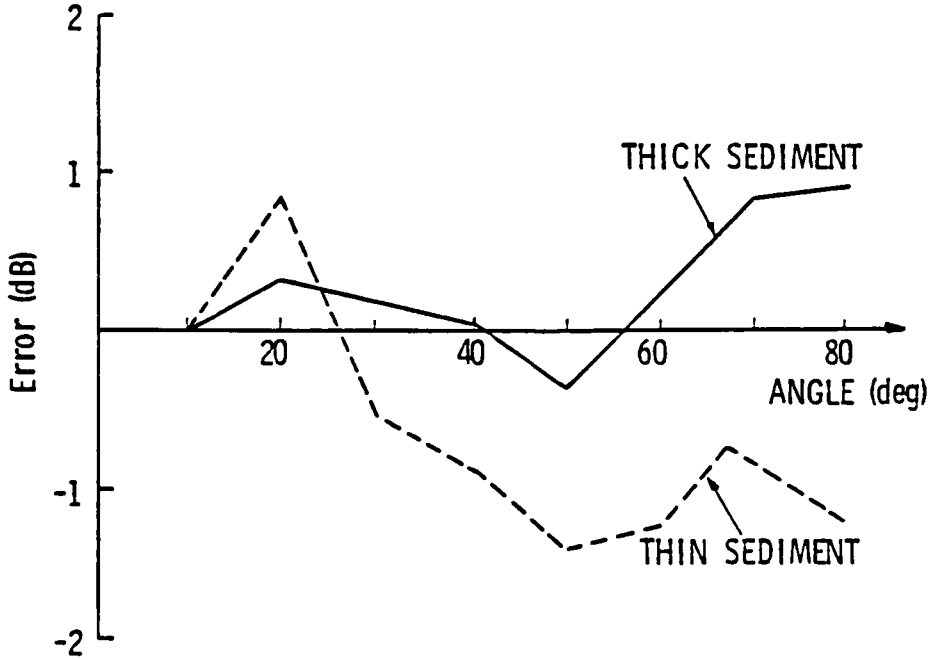


ERROR (FULL MODEL - CLOSED FORM), dB

**Figure 16** **Errors for the Assumed Case**

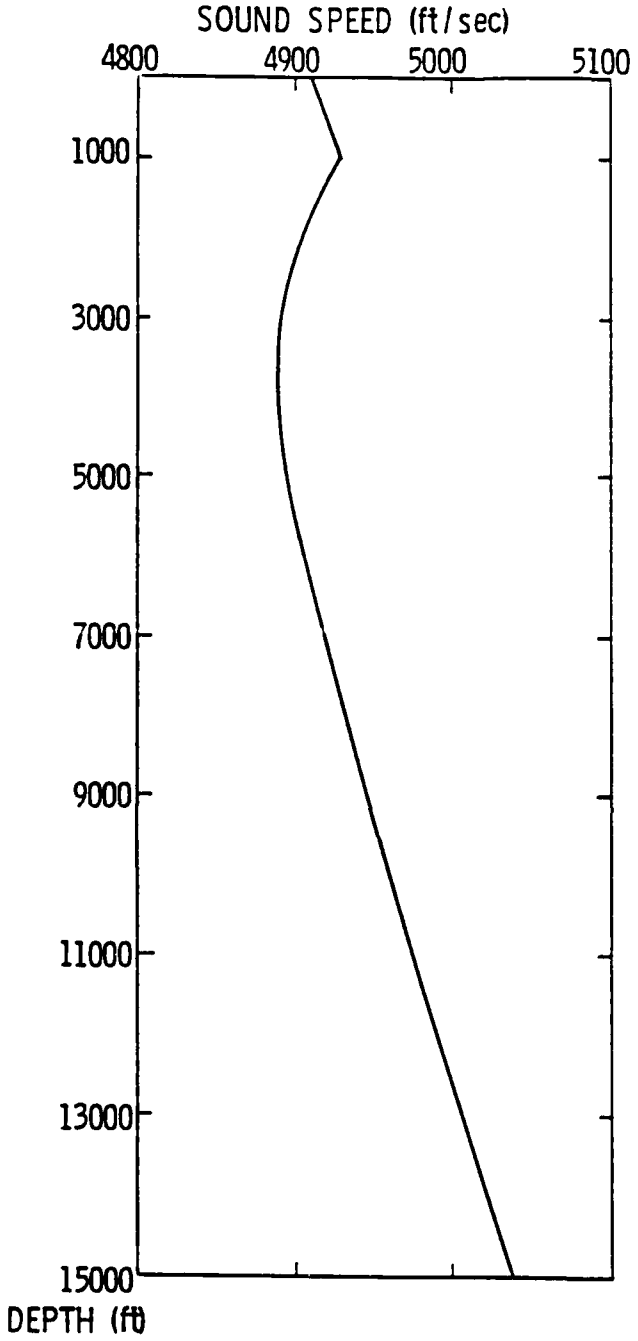


| DEPTH | SPEED |
|---|---|
| 0.0 | 4909.00 |
| 60.0 | 4910.02 |
| 325.0 | 4914.52 |
| 650.0 | 4920.05 |
| 1000.0 | 4926.00 |
| 1500.0 | 4916.00 |
| 2000.0 | 4908.00 |
| 2500.0 | 4896.00 |
| 3000.0 | 4892.00 |
| 3500.0 | 4890.00 |
| 4000.0 | 4891.00 |
| 5000.0 | 4894.00 |
| 6000.0 | 4908.00 |
| 7000.0 | 4920.00 |
| 9000.0 | 4950.00 |
| 11000.0 | 4980.00 |
| 13000.0 | 5010.00 |
| 15000.0 | 5030.00 |

Figure 17 Sound Velocity Profile

| THICK SEDIMENT (400 YDS) | | | THIN SEDIMENT (40 YDS) | | |
|---|---|---|---|---|---|
| Angle | Full Model | Closed Form | Angle | Full Model | Closed Form |
| 10 | 0.0005 | 0.0000 | 10 | 0.0005 | 0.0000 |
| 20 | 1.2067 | 0.9188 | 20 | 2.5726 | 1.7438 |
| 30 | 2.6771 | 2.6642 | 30 | 6.6305 | 7.0399 |
| 40 | 3.8927 | 3.7808 | 40 | 8.6316 | 9.2608 |
| 50 | 6.0069 | 6.2074 | 50 | 10.6117 | 11.5691 |
| 60 | 6.3189 | 6.7641 | 60 | 10.7686 | 12.3069 |
| 70 | 7.1823 | 7.1229 | 70 | 11.5598 | 12.6123 |
| 80 | 8.4251 | 7.3087 | 80 | 11.7416 | 12.4804 |

FREQUENCY LOSS (dB)

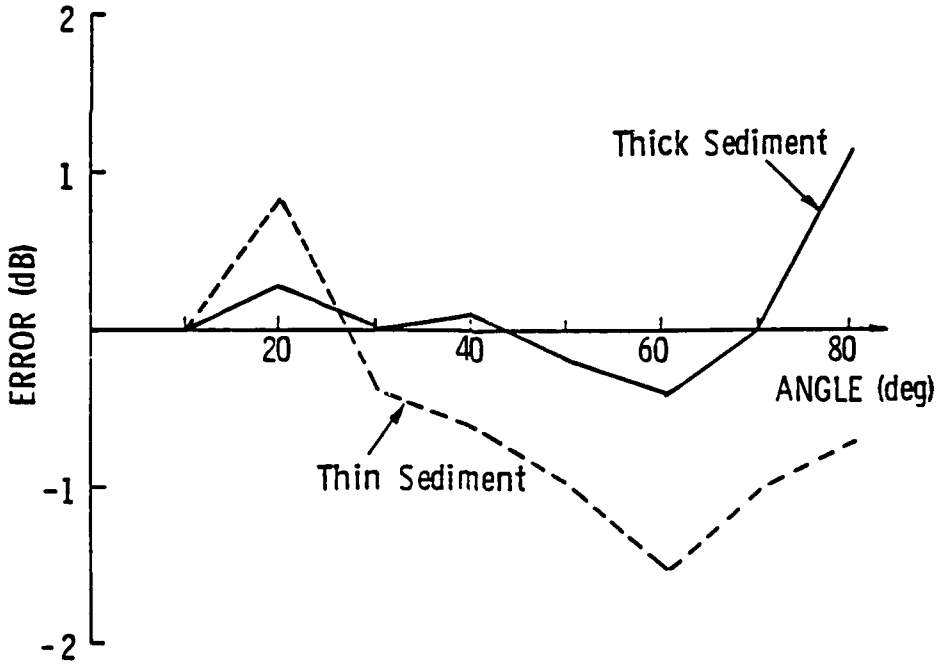


ERROR (FULL MODEL - CLOSED FORM), dB

**Figure 18** **Errors with Water SVP Introduced**

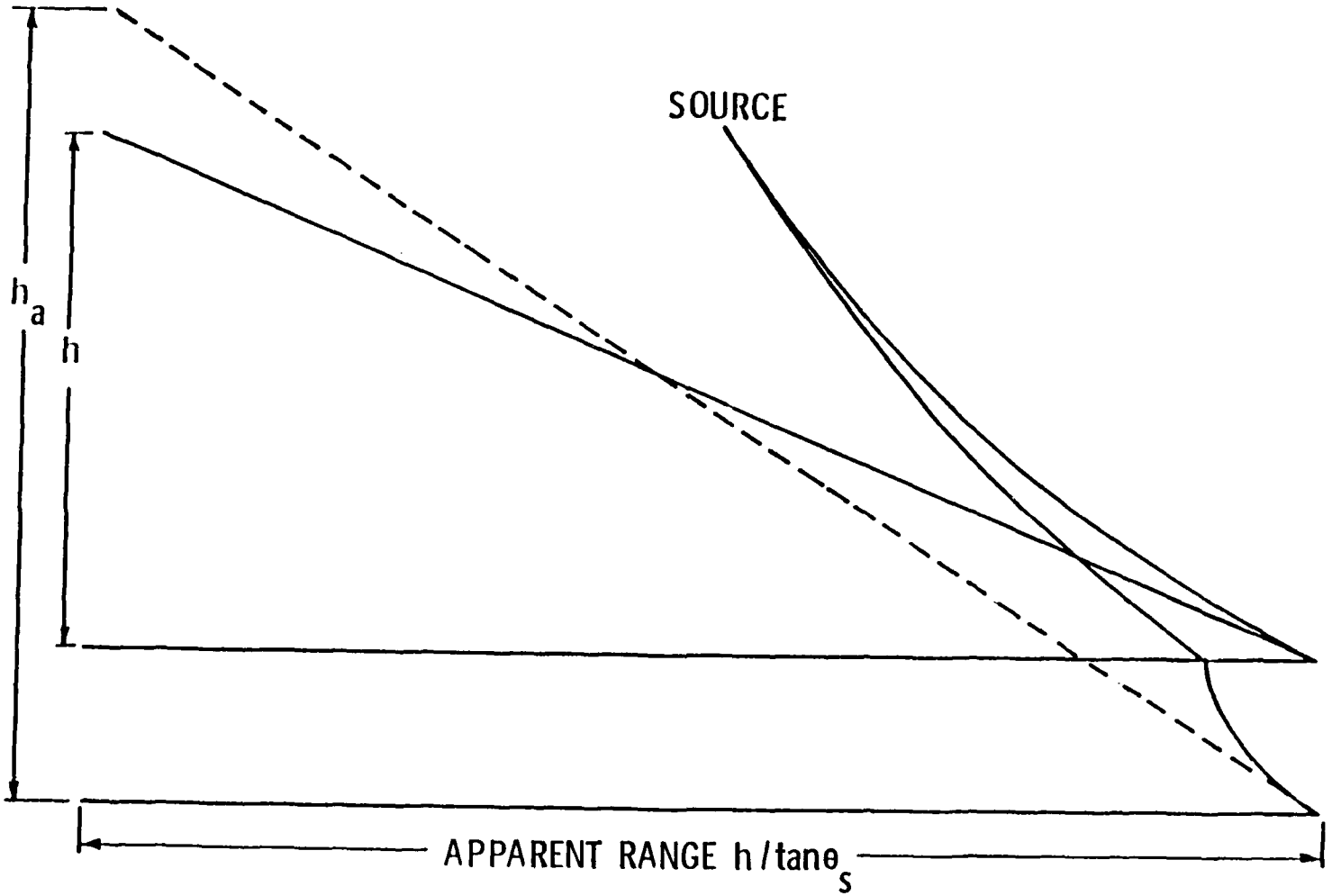


Figure 19 Illustration of Apparent Range and Height

THICK SEDIMENT (400 YDS)

| Angle | Full Model | Closed Form |
|---|---|---|
| 10 | 0.0005 | 0.0000 |
| 20 | 1.1169 | .8331 |
| 30 | 2.2681 | 2.5609 |
| 40 | 3.3644 | 3.7109 |
| 50 | 5.6380 | 6.1269 |
| 60 | 5.9329 | 6.6905 |
| 70 | 6.9211 | 7.0474 |
| 80 | 7.9117 | 7.2270 |

THIN SEDIMENT (40 YDS)

| Angle | Full Model | Closed Form |
|---|---|---|
| 10 | 0.0005 | 0.0000 |
| 20 | 1.1169 | 1.6222 |
| 30 | 5.2938 | 6.9252 |
| 40 | 8.2442 | 9.1742 |
| 50 | 10.1879 | 11.4776 |
| 60 | 10.7874 | 12.2222 |
| 70 | 11.3718 | 12.5270 |
| 80 | 11.5665 | 12.3904 |

FREQUENCY LOSS (dB)

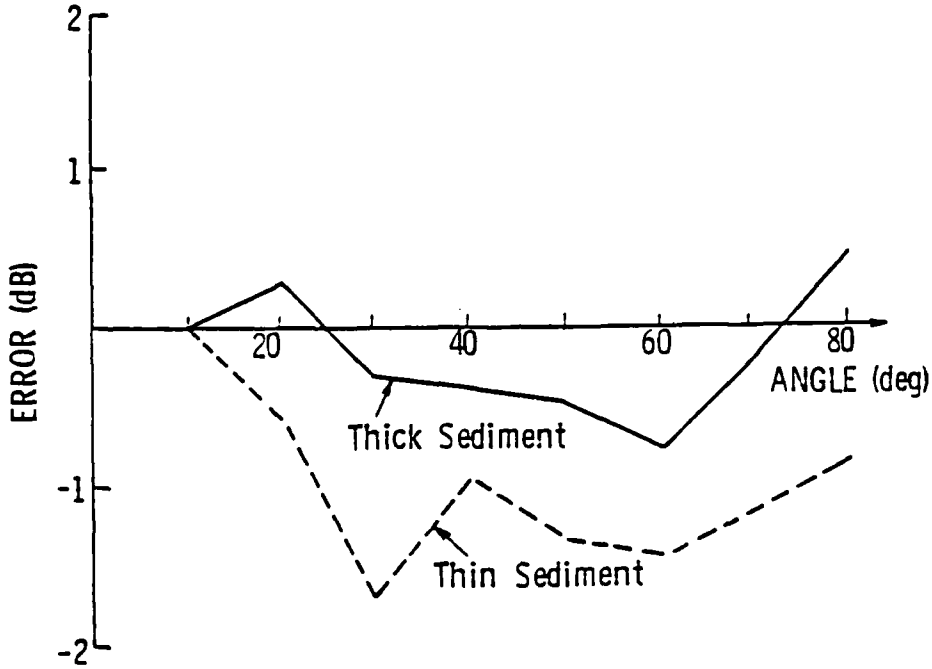


ERROR (FULL MODEL - CLOSED FORM), dB

Figure 20 Errors with Water and Sediment SVP's

THICK SEDIMENT (400 YDS)

| Angle | Full Model | Closed Form |
|---|---|---|
| 10 | 0.0003 | 0.0000 |
| 20 | 1.0942 | 0.8373 |
| 30 | 2.1179 | 2.5666 |
| 40 | 3.1042 | 3.7172 |
| 50 | 5.8210 | 6.1335 |
| 60 | 6.0133 | 6.6972 |
| 70 | 7.1507 | 7.0541 |
| 80 | 6.1600 | 7.2337 |

THIN SEDIMENT (40 YDS)

| Angle | Full Model | Closed Form |
|---|---|---|
| 10 | 0.0003 | 0.0006 |
| 20 | 1.0942 | 1.6231 |
| 30 | 5.1116 | 6.9280 |
| 40 | 7.8053 | 9.1782 |
| 50 | 10.0497 | 11.4812 |
| 60 | 10.5838 | 12.2266 |
| 70 | 10.7558 | 12.5314 |
| 80 | 10.6462 | 12.3948 |

FREQUENCY LOSS (dB)

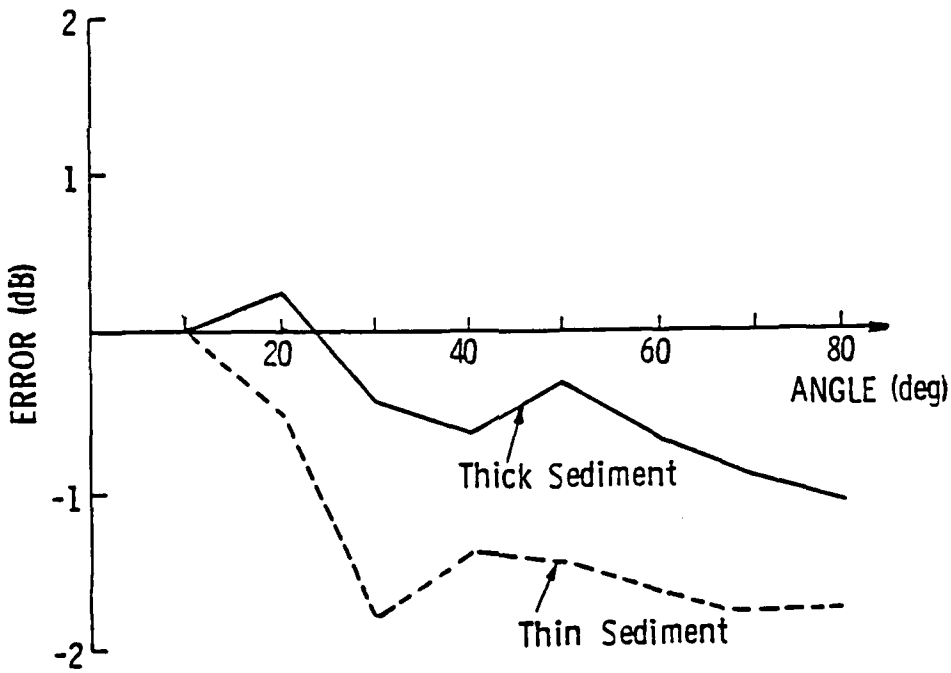


ERROR (FULL MODEL - CLOSED FORM). dB

Figure 21 Errors with Water and Sediment SVP's and Source and Receiver Offset (Source: 100 yds, Receiver: 600 yds)

| THICK SEDIMENT (400 YDS) | | | THIN SEDIMENT (40 YDS) | | |
|---|---|---|---|---|---|
| Angle | Full Model | Closed Form | Angle | Full Model | Closed Form |
| 10 | 0.0001 | 0.0000 | 10 | 0.0001 | 0.0000 |
| 20 | 0.8808 | 0.8776 | 20 | 0.8808 | 0.7751 |
| 30 | 2.1937 | 2.6267 | 30 | 5.3325 | 7.0768 |
| 40 | 3.2721 | 3.7794 | 40 | 7.5981 | 9.3076 |
| 50 | 6.2073 | 6.2002 | 50 | 10.8821 | 11.6180 |
| 60 | 6.3543 | 6.7639 | 60 | 11.4587 | 12.3576 |
| 70 | 6.4311 | 7.1210 | 70 | 11.4935 | 12.6628 |
| 80 | 6.5106 | 7.3004 | 80 | 10.9034 | 12.5280 |

FREQUENCY LOSS (dB)

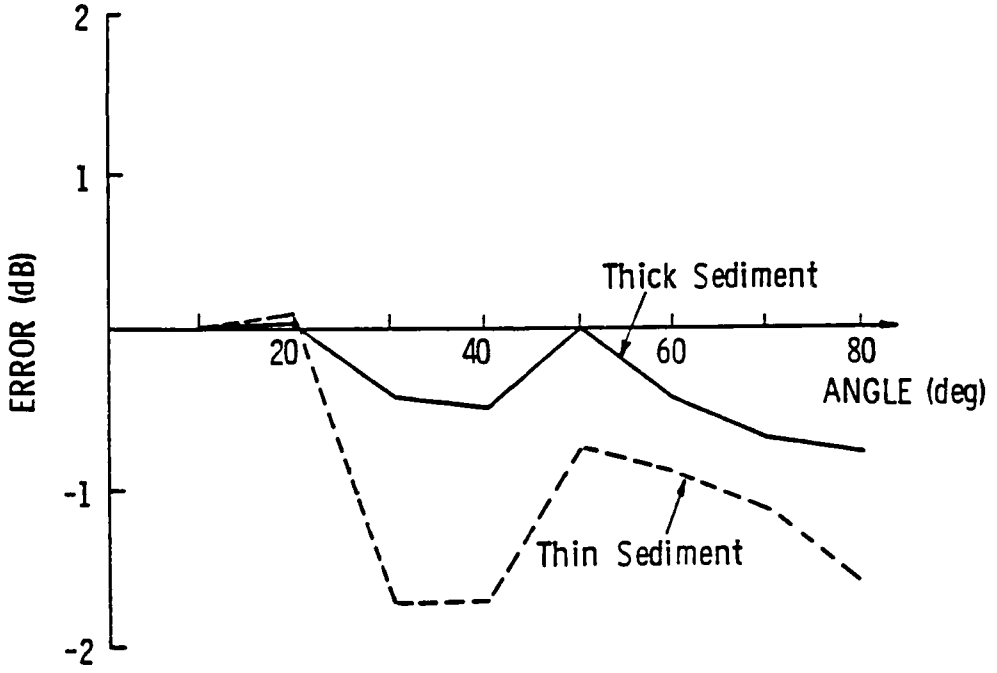


ERROR (FULL MODEL - CLOSED FORM). dB

**Figure 22** Errors with Cross-Duct Source-Reciever Positions and Shallow Water and Sediment SVP

# Chapter 4

# THE RESULTS

## 4.1. Introduction

Now that a closed form solution for the loss has been found, it is desirable to look at the final solution and see what factors most influence the loss and how.

Throughout this work, the values used for sediment density, sediment sound speed, and sediment thicknesses were take from the BLUG (Bottom Loss Up Grade) data base [3]. Some of these numbers, especially the sediment density ratio values $\rho$, are significantly different from those reported by Hamilton [5] and others. This is due to the empirical nature of the BLUG data. The sea floor parameters were used to fit a geo-acoustic model of the sea floor to measured bottom losses, and are at times unrealistic [6]. It is felt that they model the behaviour of the bottom reasonably well for the full model used here. A table of sediment properties and their ranges is now given.

| Sediment Parameter, symbol | Range of Values |
|---|---|
| Thickness,s | 40 to 2200 yards |
| Attenuation, $\alpha_s$ | 0.007 to 0.030 |
| Sound Speed Ratio, $\chi$ | 0.998 to 1.04 |
| Density Ratio, $\rho$ | 1.6 to 4.0 |

**Table 1. Sediment Parameters**

## 4.2. The Environmental Effects

By definition, the loss will be high whenever the total area that reflects significant sound back to the source is larger than the area that the receiver can detect. For a given source speed and filter bandwidth, the points the receiver can detect remain approximately the same. So the loss is therefore governed mainly by the size of the area that returns significant sound. As far as the approximate solution is concerned, that area is governed by the RMS slope of the surface doing

the scattering. For the sediment, these numbers correspond to RMS slopes of 1-6 degrees. For the rocky basement, the RMS slope is approximately 20 degrees. The higher roughness fo the basement means that sound is returned from a much larger area on the bottom for the basement path than for the sediment path. This is intuitively obvious. If the limits in $x, y$ imposed by the frequency limitations of the receiver are about the same for the basement and sediment, then a much smaller fraction of the basement energy will be detected than for the sediment path. Thus, one would expect that the loss will be high whenever the ratio of basement energy to total energy returned is large. The total energy returned is the denominator of equation 30,

$$R_s + D(1 - R_s)^2 R_b.$$

The second term represents that part of the energy returned which is due to the basement path. Thus, the ratio of basement energy to total energy will be high when the second term dominates, or when

- the total dissipation, $D$ is high
- the sediment reflection coefficient, $R_s$ is low, and
- the reflection coefficient of the basement, $R_b$, is high.

Looking first at the behavior of the dissipation ratio D, which is given by

$$D = 10^{-2s\alpha_s/\sin(\theta_b)}$$

where $2s\sin(\theta_b)$ represents the total path length in the sediment at the specular point and $\alpha_s$ is the absorption coefficient of the sediment. We can see that the dissipation ratio approaches its maximum value of unity as $2s\alpha_s/\sin(\theta_b)$ approaches zero. $\mathrm{Sin}(\theta_b)$ ranges from zero to unity, so the argument of the exponential ranges from $-\infty$ to $-2s\alpha_s$. As $\theta_b$ grows small, the argument of the exponential gets very negative, and $D$ approaches zero. Assume that

$$\theta_b \sim \arccos\left(\frac{c_w}{c_s}\cos(\theta_s)\right).$$

In the BLUG data base, the sound speed of the sediment is always expressed as a ratio to that of the water above it, $c_w/c_s$, and that ratio ($\chi$) ranges from about .998 to 1.04. So a critical angle usually exists. Below this critical angle, $\theta_b$=0, and the dissipation ratio $D$ is zero. Above the critical angle, $\theta_b$ is not zero, and the argument in the exponent approaches $2s\alpha_s$. At low angles, the basement path returns little or no energy, because the path length in the sediment is very long. Much absorption occurs, resulting in a very small dissipation ratio. This accounts for the low losses calculated for low specular angles. At high specular angles, the total path length approaches twice the sediment depth. Thus, the dissipation ratio will be small if the sediment is very thick, and larger for thinner sediments. The BLUG data base allows for sediment between 40 yards and 2200 yards deep. $\alpha_s$ ranges from .007 to .038 nepers/yard. Thus, for thinner sediments and lower $\alpha_s$, the dissipation ratio approaches unity. In these areas, higher losses at higher specular angles could take place.

The reflection coefficient is governed by two environmental parameters: sound speed ratio $\chi$, and density ratio $\rho$. Like the sediment sound speed, the sediment density is expressed as a ratio to the density of the water above it, and in the BLUG data base, that ratio ranges from 1.6 to 4.0, roughly. This is twice the range reported by Hamilton [5]. Due to the empirical nature of the BLUG data base, Spofford [6] reports artificial values as high as 6.0 in order to account for the high reflectivity of some sediments. This is artificially high, and Spofford acknowledges this. However, if good modeling of the reflectivity of the sediment is hoped for, these artificially high values serve the purpose. At low angles ($< 20°$), the reflection coefficient is governed mainly by the sound speed ratio $c_s/c_w$. This is because the sound speed ratio determines the location of the critical angle, below which perfect reflection occurs, and it is this feature of the curve which dominates low angle behaviour of the reflection coefficient. At

high angles, the density ratio $\rho_s/\rho_w$ dominates. This is because the range of the sound speed ratio is much smaller than that of the density ratio. In the BLUG data base, sound speed ratios range from 1.04 to 1.6, where the density ratios range from 1.6 to 4.0. Plots of reflection coefficient curves will show that they remain relatively constant for high enough angles ($> 30°$), and this constant is determined in large part by the density ratio. For high losses to occur, the reflection coefficient of the sediment must be low. So we can expect high losses when the specular angle is high and the density is low. At low angles, the critical angle prevents high losses from taking place.

It should be noted that at high angles, it is the action of the reflection coefficient that dominate over the effects of the absorption. If the reflection coefficient is near one, the properties of the sediment are inconsequential, as no sound returns from the basement path anyway. Only when significant transmission at the water/sediment interface takes place does increased dissipation ratio due to the thin sediment lead to higher loss.

The reflection coefficient of the basement is not a well understood quantity because of the difficulty of making measurements of the basement properties. A constant value of 0.25 was used here. If the reflection coefficient of the basement were higher, then the losses would be much higher.

Now lets look at a group of loss curves generated by the approximate solution (Figure 23, p. 58). These curves were run with a set of sediment parameters spanning the BLUG parameters: $\rho_s/\rho_w = 1.6, 4.0$, $c_s/c_w = .998, 1.04$ and $s = 40,400$ yards. The attenuation coefficient $\alpha_s$ was a constant 0.007, the lowest value generally found in the BLUG data base. Note that the lower set of curves correspond to the higher density. This is due to the higher sediment reflection coefficient, as expected. At low angles, the losses almost always tend to zero because of the increased absorption and the high reflection coefficient below the

critical angle. There is one exception, line 8. The closed form approximation assumes isovelocity velocity in the sediment,so there is no critical angle. Also, the sediment is so thin that little absorption takes place, so the dissipation ratio is high enough to allow for some loss even at 10°.

### 3.3. The System Effects

The system only controls the loss in one way for this derivation: through the filter bandwidth. Obviously for wide bandwidths, the loss will be small. For instance, for a $\Delta f$ of 0.0032, we can expect at most 3 dB of loss. In our case, with a $\Delta f$ of 0.0001, for a total bandwidth of 0.0002, we predict losses as high as 13 dB.

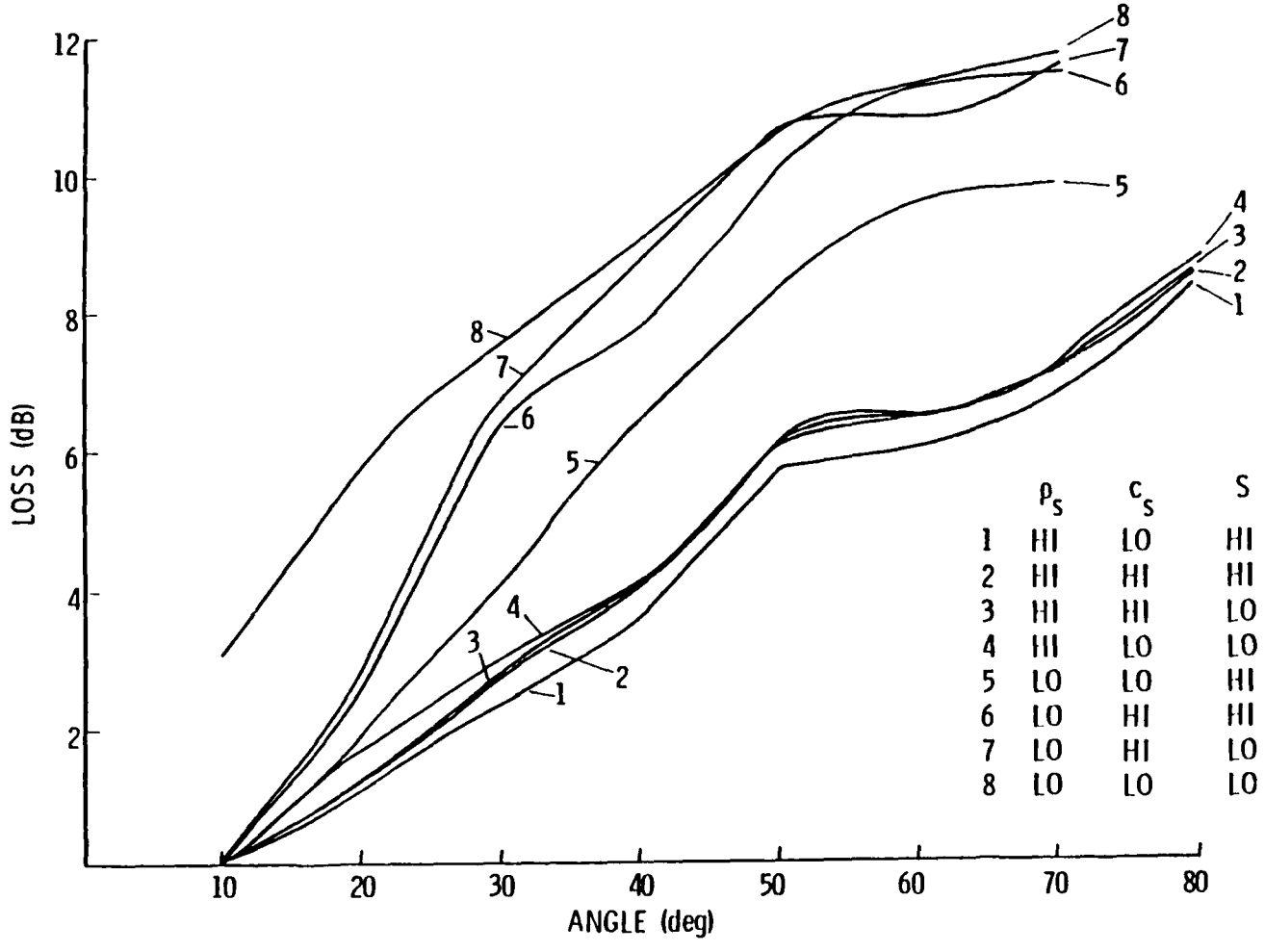


**Figure 23** System Loss Curves for Different Environments
$\rho = 1.04, 4.0$, $\chi = 0.998, 1.04$, $s = 40, 400$ yards

# Chapter 5

# THE CONCLUSIONS

## 5.1. The Conclusions

For the case of a stationary, omnidirectional receiver and an approaching, moving source, the frequency loss may be approximated by

$$L_s = \frac{R_s f(L_1, L_2, L_3) + DR_b(1 - R_s)^2 g(M_1, M_2, M_3)}{R_s + DR_b(1 - R_s)^2}, \tag{30}$$

where

$$f(L_1, L_2, L_3) = 2\sin(A_2 L_3)(\sin(A_1 L_2) - \sin(A_1 L_1)),$$

$$g(M_1, M_2, M_3) = 2\sin(A_4 M_3)(\sin(A_3 M_2) - \sin(A_3 M_1)),$$

$$A_1 = \frac{h^2 \mathrm{acos}(1/e)}{\sigma_s(h^2+R^2)}, \qquad A_3 = \frac{S_{xb}|_{x=R}}{R\sigma_b},$$

$$S_{xb}\,|_{x=R} = \frac{R}{h_a}\frac{\sqrt{4R^2+h_a^2}-h_a}{\sqrt{4R^2+h_a^2}+h_a} + \frac{R}{h_a},$$

$$R = \frac{h}{\tan(\theta_s)}, \qquad h_a \approx \frac{c_w}{c_s}h + s,$$

$$A_2 = \frac{\mathrm{acos}(1/e)}{h\sigma_s}, \qquad A_4 = \frac{\mathrm{acos}(1/e)}{h_a\sigma_b},$$

$$R_s = \left(\frac{\rho_s c_s \sin(\theta_s) - \rho_w c_w \sin(\theta_b)}{\rho_s c_s \sin(\theta_s) + \rho_w c_w \sin(\theta_b)}\right)^2,$$

$$L_1 = \max\left(\frac{-\pi}{2A_1}, -R + \sqrt{\frac{h^2}{(\cos(\theta_s + c_w)\Delta f/v_s)^2} - 1}\right),$$

$$L_2 = \min\left(\frac{\pi}{2A_1}, -R + \sqrt{\frac{h^2}{(\cos(\theta_s - c_w)\Delta f/v_s)^2} - 1}\right),$$

$$L_3 = \min\left(\frac{\pi}{2A_2}, \sqrt{(\frac{R}{c_w\Delta f/v_s - \cos(\theta_s)})^2 + R^2 + h^2}\right),$$

$$M_1 = \max\left(\frac{-\pi}{2A_3}, -R + \sqrt{\frac{h_a^2}{(\cos(\theta_b) + c_s\Delta f/v_s)^2} - 1}\right),$$

$$M_2 = \min\left(\frac{\pi}{2A_3}, -R + \sqrt{\frac{h_a^2}{(\cos(\theta_b) - c_s\Delta f/v_s)^2} - 1}\right),$$

$$M_3 = \min\left(\frac{\pi}{2A_4}, \sqrt{(\frac{R}{c_s\Delta f/v_s - \cos(\theta_b)})^2 + R^2 + h_a^2}\right).$$

This equation agrees with a much more complete, numerically evaluated model to within 2 dB for a frequency window ratio of 0.0002. It should be good whenever the frequency is not too high (< 5000 Hz), when the bottom can be modelled as a rough, hard basement covered by a sediment, and when the water is reasonably deep (>2000 feet).

## 5.2. Areas for Further Research

The possibilities for this type of analysis to be expanded to more complex problems is great. The first type of analysis that comes to mind is to estimate losses due to beam pattern limiting. If the projection of the beam onto the bottom can be delineated as simple lines or regions bounded by lines, then the method remains the same as far as the weighting functions go. The limits on the integral will do the changing for us. Once they are approximated as simple lines, then the integration is closed form, and the equations, though messy, could be evaluated on a hand calculator. Their accuracy will depend mostly on the ability of the beam pattern on the bottom to be delineated by polygons.

Time limiting should also be very amenable to these weighting functions, as time limits generate ellipses on the bottom, and are thus better fitted than frequency analysis to being depicted as boxes. As far as the area on the bottom, the frequency limitation is the most difficult loss to model.

This analysis could be taken to more layers. As a first approximation to volume reverberation in the sediment, simply adding more terms to the top of

equation (30), each corresponding to a different layer, might suffice. Their sound speeds can be different, generating a different apparent height for each layer. The tricky part would be determining their densities and roughnesses, although simple linear interpolation might suffice. Of course, with each layer, the equations will get more and more complicated. However, if even a small laptop computer is available, the possibilities are endless, as the math so far is very fast when implemented.

Some research should be done into the effect of having the source moving with a bearing other than 0 degrees. No attempt was made to test the closed form solution against sources with a component of velocity perpendicular to the source-receiver line.

# REFERENCES


1. X. Zabal, M. H. Brill and S. L. Adams, Time Spread of Acoustic Signals Reflected From a Fixed Rough Boundary, Journal of the Acoustical Society of America 75 (April,1984), 1062-1070.

2. X. Zabal, M. H. Brill and J. L. Collins, Frequency and Angle Spreads of Acoustic Signals Reflecting from a Fixed Rough Boundary, Journal of the Acoustical Society of America 79 (March 1986), 673-680.

3. Diana F. McCammon, Fundamental Relationships Between Geoacoustic Parameters and Predicted Bottom Loss Using a Thin Layer Model, to appear in Journal of Geophysical Reasearch - Oceans,1988.

4. J. J. Martin,Time and Frequency Characteristics of an Acoustic Signal Reflected from a Rough Boundary, Journal of the Acoustical Society of America 43 (1968), 405-416.

5. E. L. Hamilton,Prediction of In-Situ Acoustic and Elastic Properties of Marine Sediments,Geophysics 36 (April 1971), 266-284.

6. C. W. Spofford, R. R. Greene and J. B. Hersey,The Estimation of Geo-Acoustic Ocean Sediment Parameters From Measured Bottom Loss Data, Report Prepared for M. A. McCallister, NORDA (March, 1983).

# APPENDIX A

## DERIVATION OF THE X- AND Y-SLOPE EQUATIONS

Referring to Figure (A1), we introduce at the point of interest, $(x, y)$ a coordinate system $\psi, \eta, \varsigma$. In the terminology of vector systems this is Euclidean 3-space $E_3$. The ray path of the incident ray is represented by a unit ray at the point $(x, y)$ (See Figure (A1)). The components of this vector, called $\vec{\chi_i}$ are the projections $\psi_i, \eta_i, \varsigma_i$ onto the axes, which are the scalar products of the components with the three orthonormal basis vectors, the three unit vectors in the $\psi, \eta, \varsigma$ directions. In terms of the angles shown, the vector $\vec{\chi_i}$ is completely defined by

$$\vec{\chi_i} = \begin{pmatrix} \psi_i \\ \eta_i \\ \varsigma_i \end{pmatrix} = \begin{pmatrix} -\cos(\theta_1)\cos(\phi_1) \\ \cos(\theta_1)\sin(\phi_1) \\ \sin(\theta_1) \end{pmatrix}.$$

You'll notice $\mid \vec{\chi_i} \mid = 1$.

Similarly the direction of the reflected ray path at the point $(x, y)$ is defined by a vector $\vec{\chi_r}$ as shown in Figure (A1) and calculated below

$$\vec{\chi_r} = \begin{pmatrix} \psi_r \\ \eta_r \\ \varsigma_r \end{pmatrix} = \begin{pmatrix} \cos(\theta_2)\cos(\phi_2) \\ \cos(\theta_2)\sin(\phi_2) \\ \sin(\theta_2) \end{pmatrix}.$$

Again $\mid \vec{\chi_r} \mid = 1$.

$\vec{\chi_i}$ and $\vec{\chi_r}$ define a plane. The normal to the section of the bottom causing the specular reflection is in this plane. Denote the unit vector in the direction of the normal by $\vec{N}$. Then

$$\vec{N} = \alpha\vec{\chi_i} + \beta\vec{\chi_r}.$$

To define $\vec{N}$ we need to know $\alpha$ and $\beta$. The specular reflection requires that the angle of reflection and the angle of incidence are equal. Viewed from the direction perpendicular to the plane containing $\vec{\chi_i}$ and $\vec{\chi_r}$ and $\vec{N}$ the geometry is as shown in Figure (A1). It is easily seen that

$$\cos(\phi) = (\vec{N_i} \cdot \vec{\chi_i}) = \alpha + \beta(\vec{\chi_i}, \vec{\chi_r}) = (\vec{N} \cdot \vec{\chi_r}) = \alpha(\vec{\chi_i}, \vec{\chi_r}) + \beta,$$

so $\vec{N}$ is some constant times the sum of $\vec{\chi_i}$ and $\vec{\chi_r}$. Setting $\vec{N_0}$ to $\vec{\chi_i} + \vec{\chi_r}$ then

$$\vec{N} = \frac{\vec{N_0}}{|\vec{N_0}|} = \begin{pmatrix} \psi_n \\ \eta_n \\ \varsigma_n \end{pmatrix}.$$

Therefore

$$\vec{N_0} = \begin{pmatrix} -\cos(\theta_1)\cos(\phi_1) + \cos(\theta_2)\cos(\phi_2) \\ \cos(\theta_1)\sin(\phi_1) + \cos(\theta_2)\sin(\phi_2) \\ \sin(\theta_1) + \sin(\theta_2) \end{pmatrix}.$$

The slopes of the bottom can be found by determining the equation of the bottom plane. Let $\psi, \eta, \varsigma$ be any point in this plane. The vector of that point is

$$\vec{\chi} = \begin{pmatrix} \psi \\ \eta \\ \varsigma \end{pmatrix},$$

But all such vectors are normal to $\vec{N}$, so

$$(\vec{\chi} \cdot \vec{N}) = \psi \cdot \psi_n + \eta \cdot \eta_n + \varsigma \cdot \varsigma_n = 0.$$

According to figure (A1), the slopes in the $\psi, \eta$ direction, denoted $S_x$ and $S_y$ are found as follows. Solve for $\varsigma$

$$\varsigma = -(\frac{\psi_n}{\varsigma_n} \cdot \psi + \frac{\eta_n}{\varsigma_n} \cdot \eta).$$

Then

$$S_x = \frac{\partial \varsigma}{\partial \psi} = -\frac{\psi_n}{\varsigma_n},$$

and

$$S_y = \frac{\partial \varsigma}{\partial \eta} = -\frac{\eta_n}{\psi_n}.$$

Plugging in we get

$$S_x = \frac{\cos(\theta_1)\cos(\phi_1) - \cos(\theta_2)\cos(\phi_2)}{\sin(\theta_1) + \sin(\theta_2)},$$

$$S_y = \frac{\cos(\theta_1)\sin(\phi_1) + \cos(\theta_2)\sin(\phi_2)}{\sin(\theta_1) + \sin(\theta_2)}.$$

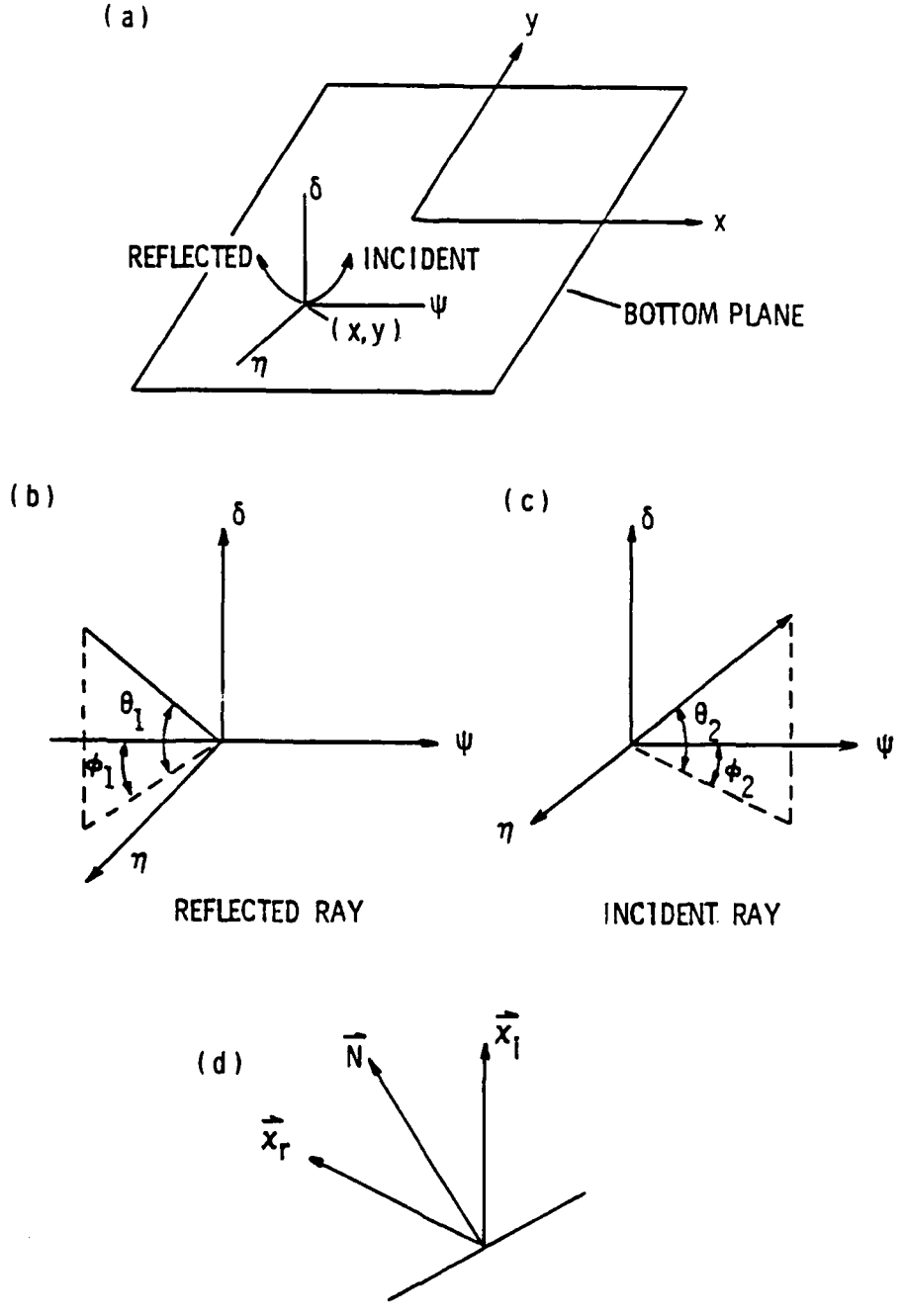


Figure A-1 Illustration of Vectors and Planes Used in Sediment Slope Calculations

# APPENDIX B

## DERIVATION OF THE LINEAR COEFFICIENT FOR SEDIMENT SLOPES

Given that

$$S_x = -\frac{R}{h}\frac{\sqrt{(R+x)^2+h^2}-\sqrt{(R-x)^2+h^2}}{\sqrt{(R+x)^2+h^2}+\sqrt{(R-x)^2+h^2}}+\frac{x}{h}.$$

Then

$$\frac{\partial S_x}{\partial x} =$$

$$-\frac{R}{h}((\sqrt{(R+x)^2+h^2}+\sqrt{(R_x)^2+h^2})\cdot(\frac{R+x}{\sqrt{(R+x)^2+h^2}}+\frac{R-x}{\sqrt{(R-x)^2+h^2}})$$

$$\frac{-(\sqrt{(R+x)^2+h^2}-\sqrt{(R-x)^2+h^2})(\frac{R+x}{\sqrt{(R+x)^2+h^2}}-\frac{R-x}{\sqrt{(R-x)^2+h^2}}))}{(\sqrt{(R+x)^2+h^2}+\sqrt{(R-x)^2+h^2})^2}+\frac{1}{h},$$

evaluated at x=0 becomes

$$-\frac{R}{h}\frac{4R}{4(R^2+h^2)}+\frac{1}{h}=\frac{h^2}{h(R^2+h^2)}=\frac{h}{R^2+h^2}.$$

# APPENDIX C

## FORMULAS FOR THE APPARENT HEIGHT

The apparent height will be used to account for refraction at the water/sediment interface. For an illustration, see Figure C1. Given the specular reflection angle off the sediment, $\theta_s$, we can calculate the total range from the source to the specular point as

$$R = \frac{h}{\tan(\theta_s)}.$$

Now, the specular basement path has the same total range, but a different angle into the sediment due to the range that gets travelled in the sediment. Summing ranges,

$$R = \frac{h}{\tan(\theta_1)} + \frac{s}{\tan(\theta_2)},$$

where $h$ is the height of the source over the ocean floor and $s$ is the depth of the sediment. If $s << h$ then $\theta_1 \approx \theta_s$ and the apparent height is given as

$$h_a \approx R \tan(\arccos(\frac{c_s}{c_w}\cos(\theta_s))).$$

The above height will always exist when needed because if we are below the critical angle, the apparent height need not be calculated.

If the range traveled in the sediment is not negligible, then the problem is somewhat complicated. Pushing forward, we know from Snell's law that

$$\frac{\cos(\theta_1)}{c_w} = \frac{\cos(\theta_2)}{c_s},$$

and from basic trigonometry

$$\tan(\theta_2) = \frac{\sqrt{1-\cos^2(\theta_2)}}{\cos(\theta_2)},$$

so that

$$\tan(\theta_1) = \frac{\sqrt{1-\frac{c_w^2}{c_s^2}\cos^2(\theta_2)}}{\frac{c_w}{c_s}\cos(\theta_2)}.$$

Plugging in, we get

$$R = h\frac{\frac{c_w}{c_s}\cos(\theta_2)}{\sqrt{1-\frac{c_w^2}{c_s^2}\cos^2(\theta_2)}} + s\frac{\cos(\theta_2)}{\sqrt{1-\cos^2(\theta_2)}}.$$

If $c_w/c_s$ is not too different from one, then we can ignore it in the denominator of the first term, yielding

$$R = \frac{hc_w}{c_s\tan(\theta_2)} + \frac{s}{\tan(\theta_2)},$$

or

$$h_a = R\tan(\theta_2) = \frac{c_w}{c_s}h + s.$$

This approximation is good for $\frac{c_w}{c_s}$ not very different from one, which happens often.

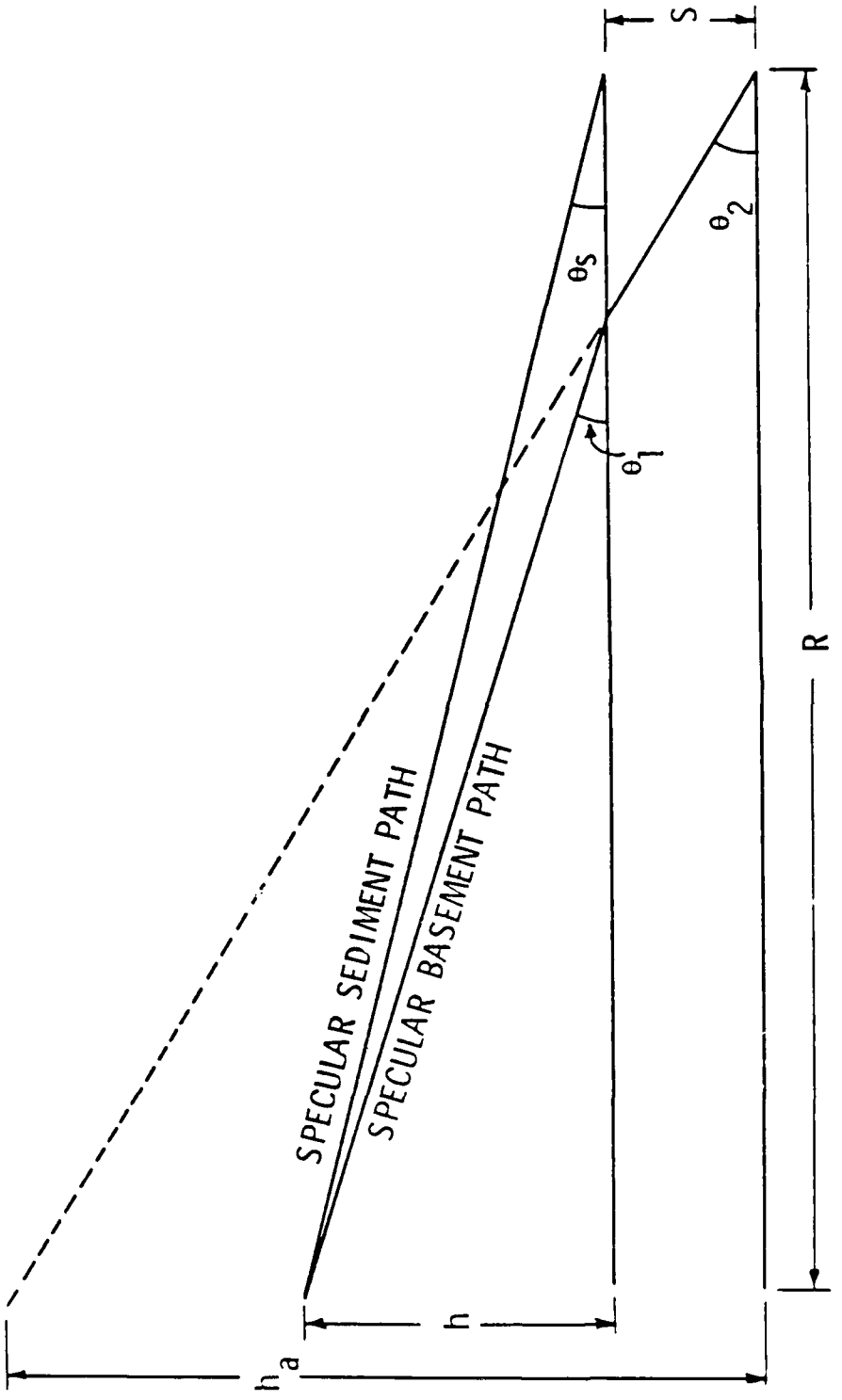


**Figure C-1 Illustration of Apparent Height**